



## Reaction paths for hydrodeoxygenation of furfuryl alcohol at TiO<sub>2</sub>/Pd interfaces



Shyam Deo <sup>a</sup>, Will Medlin <sup>b</sup>, Eranda Nikolla <sup>c</sup>, Michael J. Janik <sup>a,\*</sup>

<sup>a</sup> Department of Chemical Engineering, The Pennsylvania State University, University Park, PA 16802, United States

<sup>b</sup> Department of Chemical and Biological Engineering, University of Colorado Boulder, Boulder, CO 80303, United States

<sup>c</sup> Department of Chemical Engineering and Materials Science, Wayne State University, Detroit, MI 48202, United States

### ARTICLE INFO

#### Article history:

Received 29 April 2019

Revised 13 June 2019

Accepted 5 July 2019

Available online 26 July 2019

#### Keywords:

DFT

Furfural

Hydrodeoxygenation

Biomass

Metal-metal oxide interfaces

### ABSTRACT

Metal–metal oxide interfaces can manipulate catalytic selectivity in multistep reactions, including hydrodeoxygenation (HDO) of biomass derivatives like furfuryl alcohol. These interfaces combine active sites of different functionalities towards hydrogen activation, HDO and subsequent hydrogenation. However, examining the interplay between these different sites is essential to achieve control over the interfacial properties, and thus over the reaction selectivity towards 2-methylfuran. Herein, through DFT calculations, we investigate the role of TiO<sub>2</sub> encapsulated Pd interfacial sites towards dictating HDO product selectivity. A rutile TiO<sub>2</sub> (1 1 0) nanowire over a Pd (1 1 1) surface is used as the interfacial model. TiO<sub>2</sub>/Pd sites are found to provide a bifunctional role at the interface. The results show that TiO<sub>2</sub> generates reduced oxide sites such that C–O bond of furfuryl alcohol is activated relative to Pd (1 1 1), with the alcohol group re-oxidizing the reduced site. The Pd surface activates H<sub>2</sub> and enables hydrogenation to the final product. Consequently, deoxygenation is accelerated over a TiO<sub>2-x</sub>/Pd oxygen deficient interface, with an approximate kinetic analysis suggesting that reduced interfacial sites accelerate direct deoxygenation by ~10<sup>8</sup> at 443 K, altering the Pd selectivity from the undesired furan product to the desired 2-methylfuran.

© 2019 Elsevier Inc. All rights reserved.

### 1. Introduction

Biomass has potential as a feedstock for liquid fuels but requires processing to reduce oxygen content. Catalytic hydrodeoxygenation (HDO) generates products with suitable chemical and thermal stabilities without any loss of carbon. Biomass-derived furfural is a fuel precursor and model compound for exploring selective deoxygenation since it can undergo different reaction paths, as outlined in Fig. 1 [1]. The selective deoxygenation of furfural/furfuryl alcohol to 2-methylfuran has been studied widely [1–4], since 2-methylfuran is a potential renewable fuel component for gasoline and an intermediate in the synthesis of perfumes, medicines, and pesticides. However, the multifunctional nature (aromatic furan ring with an alcohol/aldehyde group) of these biomass-derived feedstocks necessitates selective interactions between the reactant molecules and the catalyst surface to remove the excess oxygen and to partially hydrogenate specific unsaturated groups [5]. HDO occurs through hydrogen-assisted dehydroxylation with the formation of a water molecule, whereas direct deoxygenation

(DDO) involves C–O breaking with hydrogen added afterwards to the dissociated fragments. However, over-hydrogenation and unselective C–C dissociation (decarbonylation, DCO) need to be avoided. Hence, the optimal catalyst should selectively activate the C–O bond for deoxygenation while avoiding C–C activation, as well as impart sites for subsequent hydrogenation without hydrogenating the furan ring.

Several groups have made efforts to improve the selectivity towards 2-methylfuran via supported metal catalysts of transition metals Pt, Pd, Cu or Ru over reducible oxides such as TiO<sub>2</sub> and ZrO<sub>2</sub> [5–10]. Recently core-shell catalysts, in which metal nanoparticles are coated with a shell of porous metal oxides, demonstrated improved performance in comparison with traditional supported metal catalysts [11]. Zhang et al. encapsulated palladium nanoparticles by porous TiO<sub>2</sub> and showed high selectivity and activity towards 2-methylfuran and minimal non-selective DCO, with the optimal catalyst having the smallest TiO<sub>2</sub> pore sizes [12]. Thus, cooperativity between the oxide and the metal surface at the interfacial perimeter has been proposed to enhance the selectivity to deoxygenation [13]. However, the interplay between the metal and the oxide towards enhanced deoxygenation is not understood, particularly for “inverted” systems in which the oxide partly encapsulates the metal.

\* Corresponding author.

E-mail address: [mjanik@psu.edu](mailto:mjanik@psu.edu) (M.J. Janik).

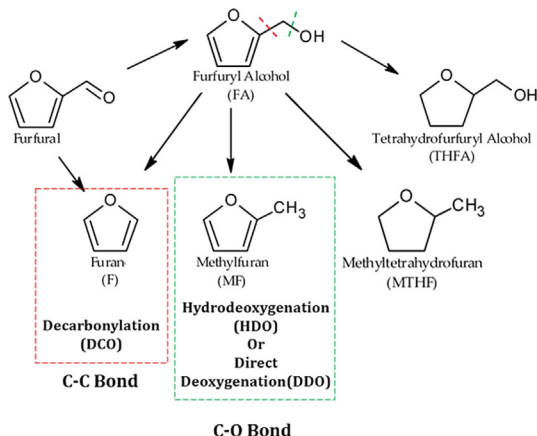


**Fig. 1.** Different reaction paths for furfuryl alcohol (reactions in green are desired while those in red are undesired). Adapted from [1].

Previous DFT and experimental studies have examined the furfural reduction mechanism and the role of metal/oxide interfacial sites [3,4,13–18]. DFT simulations over Ru/TiO<sub>2</sub> by Nelson et al. [19] have shown that TiO<sub>2</sub> can both accept a proton from H<sub>2</sub> to generate active sites and donate a proton to assist in cleaving the C—O bond of hydroxylated reactants [19]. However, other mechanisms are also possible; for example, the experimental studies of Zhang et al. [12] showed that furfuryl alcohol selectivity was correlated with more facile reduction of TiO<sub>2</sub> sites, implicating a reduction/oxidation cycle at the Pd-TiO<sub>2</sub> interface in the mechanism.

Herein, we hypothesize that reduced TiO<sub>2</sub> along the metal-oxide perimeter provides active sites that facilitate adsorption of the furfuryl oxygenates and lower the barrier for deoxygenation. These active sites, however, do not significantly affect the non-selective path of decarbonylation, thereby improving the selectivity towards deoxygenation. These hypotheses are evaluated using density functional theory (DFT) models of oxide-metal interfacial sites representing rutile TiO<sub>2</sub> on a Pd (1 1 1) surface. DFT energetics are compared with single component Pd surfaces. Our goal is to provide determination of the role of interfacial active sites towards deoxygenation and decarbonylation.

In addition to adding chemical functionality, oxide coatings may impact the structure of metal sites available to reactants and intermediates. Selectivity has been shown to be altered by effectively blocking flat-lying adsorption of ring molecules that is necessary for DCO, through steric interactions imposed by metal oxide/metal interfacial crowding in constricted TiO<sub>2</sub> pores [12] or by thiol self-assembled monolayers (SAMs) [20]. In the current study, this steric repulsion-induced selectivity over oxide-metal interfacial sites is examined through an inert helium pore DFT model over a Pd (1 1 1) surface. The pore alters the adsorption conformations of the reacting molecules. Thus, it approximates the steric crowding of adsorbates near an interface that arises out of close proximity between the metal and oxide shell within confined porosity. The effects of interfacial crowding on the deoxygenation and decarbonylation of furfuryl alcohol are compared with the effects of the chemically functional TiO<sub>2</sub>/Pd interfacial DFT model.

## 2. Computational methods

### 2.1. Electronic structure methods

Spin polarized plane-wave DFT calculations have been carried out using the Vienna Ab Initio Simulation Package (VASP), version 5.4.4. The electron-electron exchange and correlation energies are computed using the Perdew, Burke, and Ernzerhof functional [21]

with dispersion corrections, PBE-D3 [22]. The projector augmented-wave (PAW) [23] method was used to represent the ion-core electron interactions. The structural convergence criteria are 0.05 eV Å<sup>-1</sup> for all unconstrained atoms. The DFT + U method [24] within VASP has been used for Ti d states with a U<sub>eff</sub> = 2 eV to correct for on-site coulombic interaction as suggested by Hu and Metiu [25]. An optimized Pd FCC bulk lattice constant of 3.952 Å has been used for all Pd models. The plane wave energy cutoff and Monkhorst-Pack [26] k-point mesh are model specific and given in the following section. To minimize spurious interslab interactions between the periodic slabs, a vacuum space of 20 Å has been used and dipole corrections have been added in the direction perpendicular to the surface. The adsorption energy is calculated as:

$$E_{ads,molecule} = E_{molecule+surface} - E_{molecule} - E_{surface} \quad (1)$$

The gas phase energies of all molecular species have been calculated by isolating the molecule in a large unit cell. Wherever an oxygen gas phase energy is involved, the same has directly been obtained from its DFT triplet state.

### 2.2. Reaction energy and activation barrier calculations

Reaction energies for all reactions reported here have been determined by calculating the energy of all surface intermediates and gas phase molecules. In the potential energy diagrams for different reaction types, state energies are shown relative to gas phase furfuryl alcohol, the respective surface DFT model, and the appropriate stoichiometric amount of hydrogen used to balance the concerned elementary reaction step. Transition states were located using the climbing image nudged elastic band (CI-NEB) method [27] (5–7 images) and the dimer method [28] by relaxing the reaction tangent force below 0.05 eV Å<sup>-1</sup>. Transition states were verified to contain a single imaginary frequency along the reaction coordinate. Reaction energies ( $\Delta E_{rxn}$ ) and activation energies ( $\Delta E_{act}$ ) for reactions have been calculated as:

$$\Delta E_{rxn} = E_{final} - E_{initial} \quad (2)$$

$$\Delta E_{act} = E_{TS} - E_{initial} \quad (3)$$

Both these energies are ZPVE (zero-point vibrational energy) corrected.

### 2.3. Interfacial site models

#### 2.3.1. Bare Pd (1 1 1)

We compare the Pd (1 1 1) adsorption energies, associated reaction energetics and barriers with those over the metal oxide/metal interfacial DFT models to emphasize the role of the interfacial sites. A four layered 4 × 4 FCC slab was separated by 20 Å of vacuum space in the direction perpendicular to the surface (Fig. 2a). The atomic positions on the bottom two layers were frozen at their bulk lattice positions. A plane wave energy cutoff of 400 eV and a Monkhorst-Pack [26] k-point mesh of 4 × 4 × 1 were used. The high symmetry active sites for adsorption and reaction at Pd (1 1 1) include fcc hollow and hcp hollow sites for adsorption of the furfuryl rings [29]. The favorable adsorption configurations for the furanic compounds were observed to be flat conformations over an fcc hollow site. Upright configurations, with the side group towards the surface, did not experience any significant binding. The reaction energies and the activation barriers for different reaction paths over the bare Pd (1 1 1) surface agree well with those reported by Vorotnikov et al. [29], though small differences with their results are discussed.

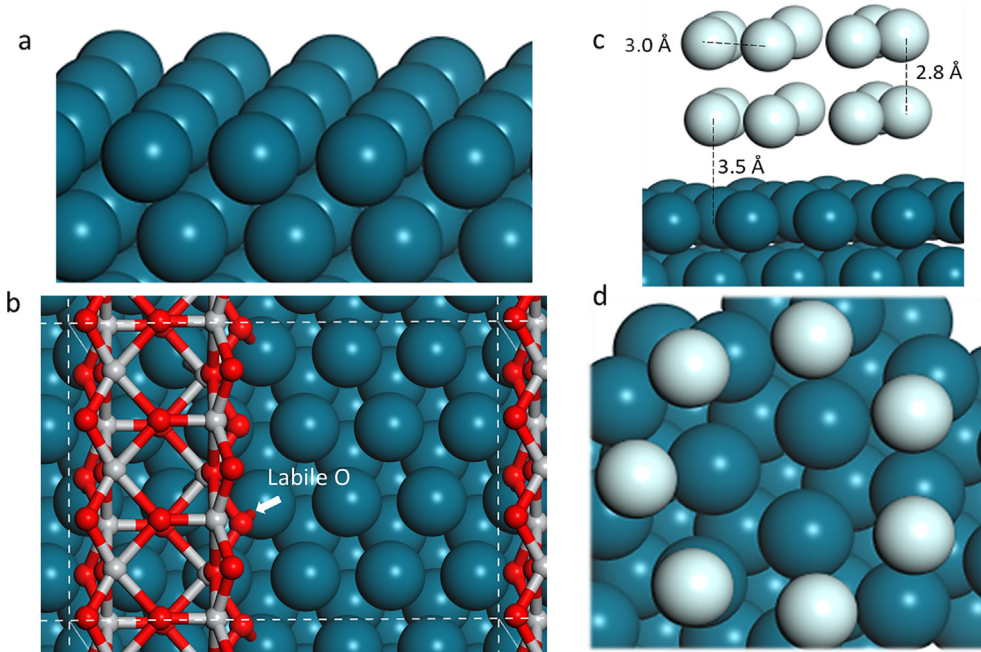


**Fig. 2.** Different DFT model systems: (a) bare Pd (1 1 1), (b) rutile-TiO<sub>2</sub> (1 1 0) nanowire over Pd (1 1 1), (c and d) inert helium pore model over Pd (1 1 1)- side view and top view.

### 2.3.2. Rutile-TiO<sub>2</sub> nanowire over the Pd (1 1 1) surface

The interfacial sites between Pd and TiO<sub>2</sub> have been represented through DFT models. The first model, which is examined most extensively, is a one-dimensional periodic rutile-TiO<sub>2</sub> nanowire adsorbed on the Pd (1 1 1) surface (Fig. 2b). This strategy for modelling the interface of a metal oxide over metal surface was guided by a similar approach used by Vandichel et al. [30] for their analyses of low temperature CO oxidation at a SnO<sub>x</sub>/Pt interface. The rod has two TiO<sub>2</sub> layers in each non-periodic direction. Each face exposes a (1 1 0) surface, both to the vacuum/adsorbates and to the metal surface. The (1 1 0) surface is the most stable facet of rutile TiO<sub>2</sub> [31]. Rutile was chosen due to its least lattice mismatch with the Pd (1 1 1) surface. The metal surface has been modelled as a 5 × 4 surface cell with four layers. The nanowire expands the rutile TiO<sub>2</sub> lattice by 8.3% in the periodic lattice direction *c*, relative to the bulk optimised lattice constants (*a* = *b* = 4.617 Å and *c* = 2.974 Å). A model with smaller strain would require a larger unit cell adding to computational cost. Nonetheless, it is assumed that this strain is small enough to only affect the absolute energy values but not our conclusions. The rod was placed at different positions on the metal surface and the lowest energy configuration was chosen for further investigations. The oxygen atom designated as *labile O* in Fig. 2b is bound to both the Pd surface and is part of the TiO<sub>2</sub> nanowire, serving as an interfacial site. A plane wave energy cutoff of 450 eV and a Monkhorst-Pack [26] k-point mesh of 2 × 3 × 1 was used for this model.

The oxygen vacancy formation energy was calculated for the interfacial oxygen atoms, defined as the energy to desorb an oxygen atom as 1/2 O<sub>2</sub> as TiO<sub>2</sub> → TiO<sub>2-x</sub> + 1/2 O<sub>2</sub>. Though oxygen desorption is not directly relevant to furfural reduction chemistry, it serves as a measure of reducibility that can be compared with other TiO<sub>2</sub> models in the literature. The oxygen vacancy formation energy for the extended rutile TiO<sub>2</sub> (1 1 0) surface is 3.56 eV, using a 3 × 1 cell to match the vacancy concentration in the nanowire. This is close to the reported value of 3.71 eV [32]. Vacancy formation is significantly more endothermic (4.46 eV) in the isolated nanowire, presumably due to the instability of edge vacancy sites that expose undercoordinated Ti atoms. When the nanowire is

adsorbed to the Pd (1 1 1) surface, interfacial vacancies are relatively stabilized by structural coordination with Pd and the associated electronic exchange [33], discussed later in Section 3.1. Consequently, the interfacial oxygen atom vacancy formation energy ranged between 3.67 and 3.74 eV. Thus, our TiO<sub>2</sub> nanowire/Pd (1 1 1) interfacial reducibility is not significantly shifted from that of rutile (1 1 0). We conclude that the constructed nanowire is a reasonable model to examine the impact of interfacial reducible sites on catalytic chemistry, without overestimating the role of O vacancies due to an unrealistic enhancement of their stability at the interface. This model has available Pd sites near the nanowire to allow planar binding of furfural derivatives, allowing direct comparison of energetics to bare Pd. For example, furfuryl alcohol adsorbed in similar conformations over a hollow fcc site has an equivalent adsorption energy of −1.87 eV over the bare Pd surface and near the interfacial sites of TiO<sub>2</sub>/Pd.

### 2.3.3. Inert helium pore model

To mimic the steric constraints that would arise from crowding near an interface or within constricted TiO<sub>2</sub>/Pd pores, we used a second DFT model – a helium pore over a four layered Pd (1 1 1) surface (Fig. 2c and d). This pore model approach has been introduced, described, and validated in detail by Gomez-Gualdrón et al. [34] for DFT study of the selective oxidation of n-butane to 1-butanol over Pd (1 1 1). This model is comprised of a pore ring consisting of inert helium atoms evenly distributed along the circumference and centered over a hollow or atop position of the metal surface. The bottom ring of the pore is above the palladium surface by 3.5 Å, while the top and bottom rings are separated by 2.8 Å. The helium-helium interatomic distances are kept at 3 Å and the number of helium atoms in the ring is varied to get the desired pore diameter. The pore diameter has been varied from 5.8 to 8 Å to provide the adsorbing molecules varying degrees of steric interactions and thereby motivating any orientation-induced selectivity for deoxygenation. Reaction energetics and activation barriers for HDO and DCO steps were computed on this pore model, which limits (or prevents) adsorption with the furyl ring parallel to the surface plane.

### 3. Results and discussion

Before we examine elementary furfuryl alcohol reactions, we must examine the stability of interfacial structures of the rutile-TiO<sub>2</sub> nanowire/Pd (1 1 1) model. Since TiO<sub>2</sub> can accept a H from H<sub>2</sub> activation, a number of different structures can form at the TiO<sub>2</sub>/Pd interface under different reaction temperatures or hydrogen partial pressures, and these are investigated in Section 3.1. Section 3.2 is then organized by individual types of reaction where we go through each of the models under the different reaction types, with the goal of determining whether the bifunctional TiO<sub>2</sub>/Pd significantly alters the rate of each reaction type. We start with direct deoxygenation, hydrodeoxygination and then decarbonylation. The role of surface crowding through the inert pore model has also been included under respective reaction types (Section 3.2) to examine site-blocking effects on the selectivity to deoxygenation over decarbonylation. After establishing in Section 3.2 that the barrier for direct deoxygenation is lowered at the reduced interfacial sites, Section 3.3 analyses the full catalytic mechanism on those sites relative to Pd (1 1 1).

Throughout our study, we have considered low coverage of hydrogen, with H\* co-adsorbed only when needed. Furfuryl alcohol and its derived intermediates were also studied at low coverage. Due to the TiO<sub>2</sub> nanowire covering portions on the Pd surface, quantifying coverage near the interface requires assumptions as to which Pd atoms are exposed and which are not. If we estimate this roughly, the coverage used is 1H per 16 Pd atoms for the TiO<sub>2</sub>/Pd interfacial models and the bare Pd (1 1 1) model. All energetics reported in this paper are also tabulated in the Supplementary Information, Table S1. Structures of all adsorbed intermediates (reactant and product states) are illustrated in Tables S2, S3 and S4.

#### 3.1. Formation of reduced active sites at the TiO<sub>2</sub>/Pd (1 1 1) interface

##### 3.1.1. Reduced Interface as TiO<sub>2</sub>-H (1 1 0)/H-Pd (1 1 1)

Under fully oxidized conditions, TiO<sub>2</sub> would expose a stoichiometric, unreduced form with all Ti atoms in the formal 4+ oxidation state. Under typical hydrogenation conditions, however, H<sub>2</sub> can dissociate spontaneously over the Pd surface [35] and adsorbed H\* would be present at the interface. H atoms can then spill over to TiO<sub>2</sub> and bind to an O<sup>2-</sup> ion forming a hydroxyl group (Fig. 3) and an electron localized on Ti that formally becomes a Ti<sup>3+</sup>. The reaction energy for the hydrogen spillover is exergonic relative to the dissociative adsorption of H<sub>2</sub> at the interface (state b relative to state a, Fig. 4) to be discussed later in the section. Hydrogen adsorption energies are similar over Pd and TiO<sub>2</sub> at the interface ( $E_{\text{ads}} = -0.20 \text{ eV}$  and  $-0.30 \text{ eV}$  to a Pd hollow site and interfacial

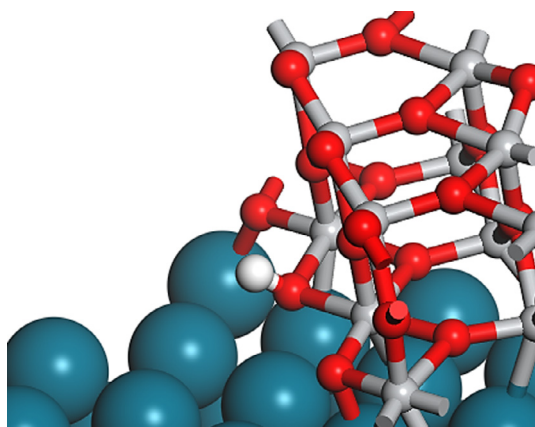


Fig. 3. Reduced interface with H adsorbed over the interface oxygen.

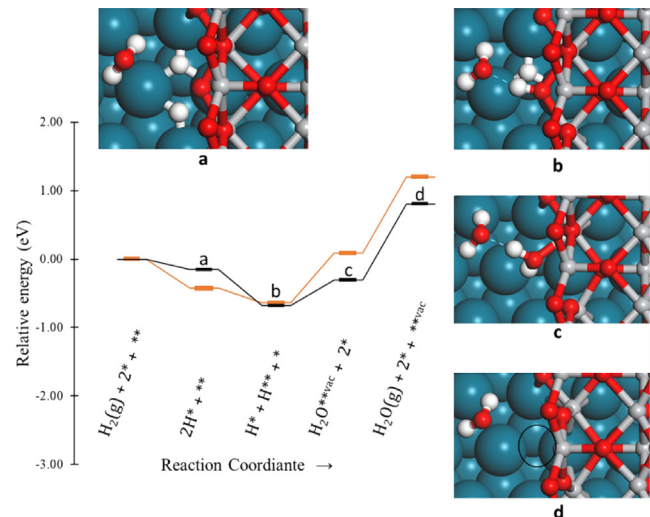


Fig. 4. Reaction scheme for hydrogen adsorbed at the interface leading to an oxygen vacancy with (-black) and without (-orange) the presence of water. Images show states along the vacancy formation process with an additional water molecule co-adsorbed. Blue dotted lines in states b and c show hydrogen bonding. \* and \*\*<sub>vac</sub> refer to Pd sites, oxygen sites of TiO<sub>2</sub> and TiO<sub>2</sub> vacancy sites at the interface respectively.

TiO<sub>2</sub> respectively). Hydrogen binding on the Pd surface away from the interface is more favorable ( $E_{\text{ads}} = -0.55 \text{ eV}$ ) and similar to the adsorption energy of hydrogen on the bare Pd (1 1 1) model ( $E_{\text{ads}} = -0.64 \text{ eV}$ ). Thus, at low chemical potentials, H is expected to reside at Pd site remote from the interface. However, at the high H<sub>2</sub> chemical potentials used in biomass upgrading reactions, hydrogen is also expected to occupy interfacial sites. The magnitude of the binding energy differences between Pd and interface sites are similar to differences observed for Pd/Cu (1 1 1) single atom alloy systems [36] in which H spills over from Pd to Cu. Likewise, under high densities of interfacial sites over the Pd surface, we can assume that H will dissociate on Pd (away from the interface) in hydrogenation environment and spill over to the TiO<sub>2</sub>/Pd interface, forming reduced Ti<sup>3+</sup> interfacial sites.

##### 3.1.2. TiO<sub>2-x</sub>/Pd Reduced Surface (O Vacancy)

An oxygen vacancy at the interface of TiO<sub>2-x</sub>/Pd may help activate the C—O bond, with oxygen from the adsorbate filling the vacancy. Hence, before examining the reaction chemistry of furfuryl alcohol hydrodeoxygination, we investigated the energetics to generate these oxygen vacancies. H<sub>2</sub> may reduce TiO<sub>2</sub> at the Pd interface to generate a water molecule and oxygen vacancy. The overall reaction is  $\text{TiO}_2 + \text{H}_2 \rightarrow \text{TiO}_{2-x} + \text{H}_2\text{O}$ . The energetics and structures involved in this process are illustrated in Fig. 4. H<sub>2</sub> first activates on the Pd surface (dissociative adsorption over adjacent hollow sites, state a, Fig. 4) and one H atom then spills over to TiO<sub>2</sub> to form a hydroxylated/reduced TiO<sub>2</sub> interface (state b, Fig. 4). The reaction energy for the first spillover is exergonic relative to dissociative H<sub>2</sub> adsorption on Pd (state b relative to state a,  $\Delta E = -0.22 \text{ eV}$  without water and  $-0.53 \text{ eV}$  with water co-adsorbed). Differing reaction energies with and without co-adsorbate indicate the spillover process to be coverage dependent. In the next step, a second H atom adsorbed on the Pd surface spills to the oxide to bind to the same O ion (state c, Fig. 4) and form the precursor state for water desorption. A higher energy transition state was not located for this spillover and the barrier is equal to the reaction energy ( $E_{\text{act}} \approx \Delta E_{\text{rxn}} \approx 0.81 \text{ eV}$ ). This barrier reduces to 0.40 eV ( $E_{\text{act}} \approx \Delta E_{\text{rxn}}$ ) due to stabilization through hydrogen bonding when a water molecule is co-adsorbed at the interface. Likewise, neighboring hydroxyls or water over TiO<sub>2</sub> at the interface

would also facilitate hydrogen transfer, forming the water precursor state. The kinetic barrier for the first hydrogen spillover to  $\text{TiO}_2$  was not examined, as it is expected to be lower than that of the second spillover due to the much negative enthalpy of reaction for the first step. Finally, removal of the water molecule from state c costs 1.11 eV, leaving behind an oxygen vacancy (state d) (Table S1, step Xb). This energy cost is consistent with the previous estimates over a rutile  $\text{TiO}_2$  (1 1 0) surface [37]. Overall, the cost to create a vacancy from the hydroxylated surface (state d relative to state a, Fig. 4) is 0.96 eV with a water molecule co-adsorbed at the interface and 1.62 eV without water co-adsorbed.

Despite the endothermicity of 1.62 eV needed to create an interfacial oxygen vacancy, this value reflects an upper limit that would be lowered if a higher coverage of hydrogen and furfural-derived intermediates was considered. Under a typical HDO reaction environment, high coverage of reaction intermediates is likely and hence the desorption cost for a water molecule would decrease due to repulsive co-adsorbate interactions. For example, the desorption energy for water is lowered by 0.37 eV near a co-adsorbed 2-methylfuran species, thereby lowering the overall cost to create an O vacancy by the same amount. Furthermore, these energetics do not include entropic effects, which would also drive the desorption due to the entropy gained through gas molecule formation. Zhang and co-workers [12] have performed temperature programmed reduction (TPR) to evaluate the reducibility of  $\text{TiO}_2$  encapsulated Pd nanoparticles. They observed the lowest onset of reduction at 160 °C. Gas phase furfuryl alcohol deoxygenation was performed at 170 °C. Thus, oxygen vacancies would be present at the  $\text{TiO}_2$  interface under furfuryl alcohol HDO conditions.

Oxygen vacancy formation creates a reduced surface, where 2 e<sup>-</sup> previously involved in Ti–O bonding are redistributed. In a pure  $\text{TiO}_2$  surface, this results in formation of two formal  $\text{Ti}^{3+}$  cations. At the interface, Bader charge analysis shows that a portion of these excess electrons is localized over the two Ti atoms adjacent to the vacancy, with an additional 0.1 e<sup>-</sup> on each Ti. A charge of 0.78 e<sup>-</sup> transfers from the oxide to the Pd surface upon vacancy formation, with 0.38 e<sup>-</sup> assigned to the Pd atom underneath the vacancy and the remaining 0.4 e<sup>-</sup> delocalized across the surface. The presence of interfacial oxygen vacancies therefore does not solely reduce Ti atoms but creates a delocalized negative charge in the Pd surface. The same is true with hydrogen spillover from Pd to create a hydrogen-adsorbed reduced interface. The Bader charges are more consistent with a proton transfer from Pd to the O of the nanowire with the associated charge delocalized among the nanowire Ti atoms and the Pd substrate. Yet the term ‘hydrogen spillover’ has been used throughout the text, which should be understood as transferring the H nuclei to bind to the nanowire and the associated negative charge delocalizing at the interface.

### 3.2. Furfuryl alcohol deoxygenation and decarbonylation key steps across different active sites

With our active site models established, we now examine the energetics of key reaction steps comparing across the different models. These include C–O bond breaking for deoxygenation (DDO), hydrogen-assisted deoxygenation (HDO), and C–C breaking for decarbonylation (DCO). We organize these analyses by reaction types, examining how key energetics are impacted by different models. We then examine the complete reaction cycle for the reaction paths that show low barriers for key reaction steps in the following sections.

#### 3.2.1. Direct deoxygenation (DDO)

Direct deoxygenation refers to cleaving of the C–OH bond of furfuryl alcohol under activation with the catalyst surface to form surface adsorbed OH<sup>\*</sup> and  $\text{C}_4\text{H}_3\text{O}(\text{CH}_2)^*$  dissociated fragments.

These fragments would then be further hydrogenated to produce water and the final desired product, 2-methylfuran. The activation barrier for the DDO step varies substantially from 0.95 eV on the bare Pd (1 1 1) surface to 0.20 eV over a reduced  $\text{TiO}_2/\text{Pd}$  interface. Potential energy surfaces (PES) of DDO paths across different DFT models are shown and compared in Fig. 5.

**3.2.1.1. Bare Pd (1 1 1):** Over the Pd (1 1 1) surface, DDO of furfuryl alcohol occurs with an activation barrier of 0.95 eV and the reaction is uphill by 0.21 eV (Fig. 5). At the transition state, the methylfuryl radical  $\text{C}_4\text{H}_3\text{O}(\text{CH}_2)^*$  is adsorbed over an fcc-hollow site and the hydroxyl group interacts with both the methyl carbon and a nearby surface bridge site (Fig. 6a). Our barrier is close to the barrier (1.05 eV) reported by Vorotnikov et al. [29] over the Pd (1 1 1) surface. The DDO barrier rises to 1.19 eV when the furfuryl alcohol and the dissociated organic fragments are adsorbed upright (Fig. 6b). The higher barrier occurs due to difficulty obtaining simultaneous formation of surface-OH and surface-CH<sub>2</sub> interactions at the transition state.

The DDO path may proceed initially through alcohol O–H dissociation, followed by C–O dissociation. The O–H dissociation barrier is equivalent to the DDO barrier of 0.94 eV but the reaction is more endothermic (0.48 eV) (Table S1, step Va). After abstraction, H is adsorbed to a hollow site on the surface. Subsequent C–O dissociation occurs with a surmountable barrier of 0.49 eV (Table S1, step VIa). This alternate path of dehydrogenation followed by C–O dissociation may be less favorable compared to DDO at higher intermediate or hydrogen coverages. This path requires two subsequent O–H formation steps to reverse the initial O–H dehydrogenation and form water.

**3.2.1.2. Rutile- $\text{TiO}_2$  nanowire over the Pd (1 1 1) surface. Stoichiometric  $\text{TiO}_2/\text{Pd}$  Interface:** The DDO step at the stoichiometric interface has a barrier of 0.91 eV, comparable to that over the Pd (1 1 1) surface. At the transition state for deoxygenation, the 2-methylfuryl radical  $\text{C}_4\text{H}_3\text{O}(\text{CH}_2)^*$  is adsorbed over a hollow site on the Pd surface and the hydroxyl group partially forms a HO–Ti bond (Fig. 6d). The reaction energy is uphill by 0.50 eV (Fig. 5), more endothermic than on Pd (1 1 1). The less favorable DDO reaction energy arises from stabilization of the initial state by the interface, not destabilization of the product state. Furfuryl alcohol adsorbs more strongly to the interface due to an additional Ti–O interaction ( $E_{\text{ads}} = -2.44$  eV at  $\text{TiO}_2/\text{Pd}$  vs  $-1.87$  eV on Pd (1 1 1)). The product state is also stabilized at the interface as OH adsorbs on the fully oxidized  $\text{TiO}_2$  nanowire 0.48 eV more strongly than OH adsorbed on Pd (1 1 1). However, the greater initial state stabilization makes DDO less favorable at the interface.

The DDO path may proceed initially through alcohol O–H dissociation followed by C–O dissociation, and this may be enabled through more favorable O–H dissociation at the interface. At the  $\text{TiO}_2/\text{Pd}$  interface, O–H dissociation has a reaction energy of 0.34 eV and a barrier of 0.52 eV (Table S1, step Vb), leaving the H adsorbed to an O atom of  $\text{TiO}_2$  and the methoxy adsorbed on Pd (Fig. 6c). The interface facilitates this step, as it is more endothermic (0.48 eV) and has a higher barrier (0.94 eV) on Pd (1 1 1). Subsequent C–O dissociation at the  $\text{TiO}_2/\text{Pd}$  interface is favorable ( $-0.67$  eV versus 0.1 eV on Pd (1 1 1)) with a surmountable barrier of 0.47 eV (0.49 eV on Pd (1 1 1)). The stoichiometric  $\text{TiO}_2/\text{Pd}$  interface may promote DDO through this path. The dehydrogenation step, however, may be less favorable at higher intermediate coverages and would require an additional subsequent hydrogenation step to form the  $\text{H}_2\text{O}$  product. We also report, below, more DDO sequences that occur over even lower barriers on reduced interfacial sites.

**Reduced Interface as  $\text{TiO}_2\text{-H/Pd-H}$ :** The barrier to DDO was studied at a reduced interface with hydrogen adsorbed on  $\text{TiO}_2$ .

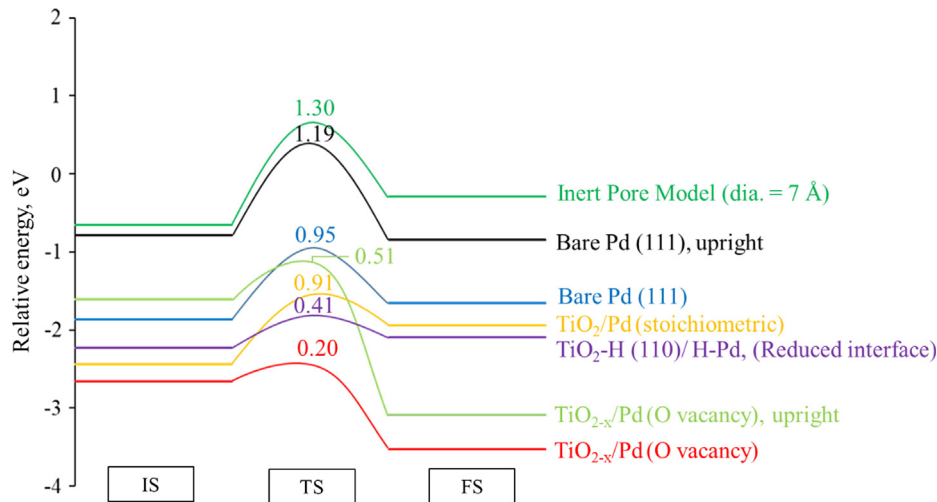


**Fig. 5.** Potential energy surfaces (PES) of DDO path over different DFT models as labelled. Initial and final state energies are plotted with respect to the energy of gas phase furfuryl alcohol and the respective surface models without adsorbed hydrocarbons. Activation energy barriers ( $E_a$ ) in electronvolts are labelled. Transition state structures are illustrated in Fig. 6.

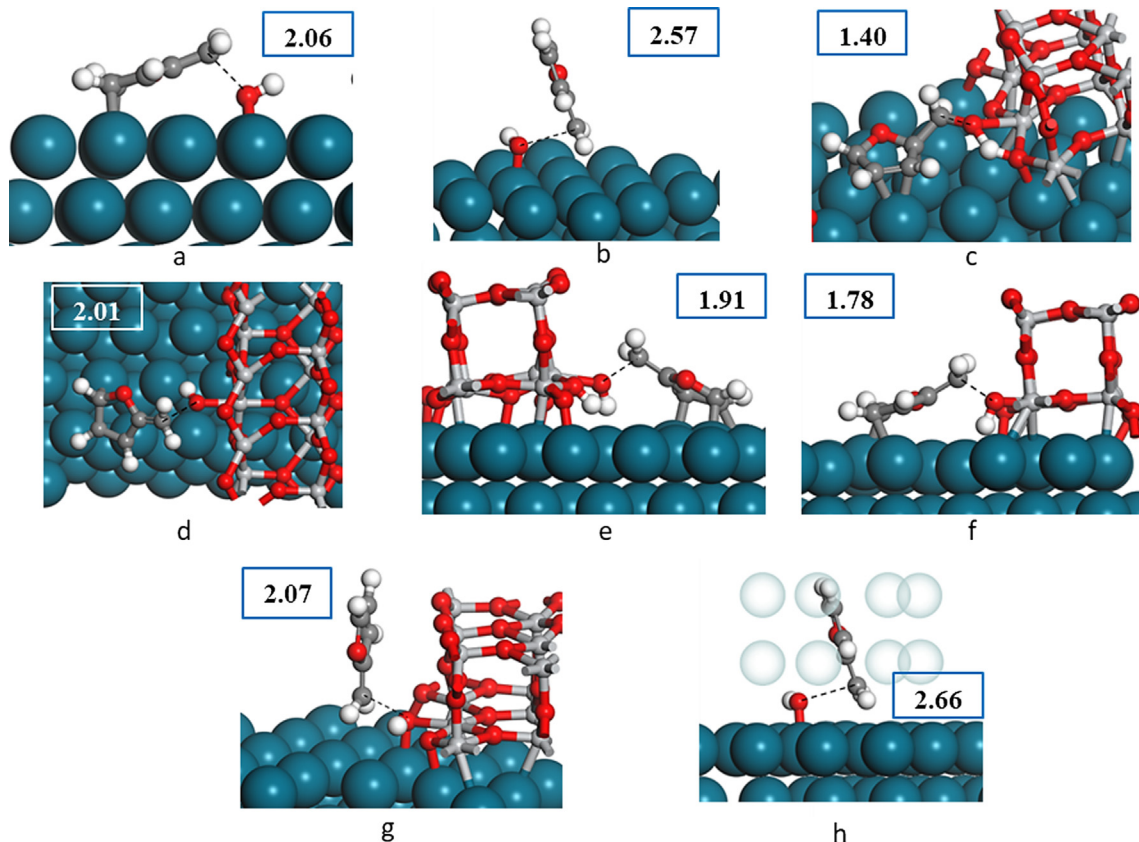


**Fig. 6.** Transition states for DDO over (a) bare Pd (1 1 1), (b) bare Pd (1 1 1) with upright conformation under steric crowding, (c) stoichiometric  $\text{TiO}_2/\text{Pd}$  with H abstraction before C–O activation, (d) stoichiometric  $\text{TiO}_2/\text{Pd}$ , (e) H- $\text{TiO}_2/\text{Pd}$  reduced interface, (f)  $\text{TiO}_{2-x}/\text{Pd}$  oxygen deficient interface, (g)  $\text{TiO}_{2-x}/\text{Pd}$  oxygen deficient interface with upright adsorption, and (h) inert pore model with pore diameter of 7 Å (helium pore atoms are shown transparent for clarity). The C–O bond distances (involved in DDO) are shown in rectangular boxes on all DFT models. Initial and final states' structures across these DFT models are tabulated in Table S2.

The adsorption of furfuryl alcohol at this interface allows the furyl ring to interact with the Pd (1 1 1) surface while the alcohol hydroxyl group interacts with  $\text{Ti}^{3+}$  by forming a Ti–OH moiety (Fig. 6e). The molecule adsorbs with an adsorption energy approximately 0.2 eV weaker than on the stoichiometric interface. At the transition state for deoxygenation, the 2-methylfuryl radical  $\text{C}_4\text{H}_3\text{O}^{\cdot}$  ( $\text{CH}_2^{\cdot}$ ) is adsorbed over a hollow site on the Pd surface (as on bare

Pd (1 1 1)), and the hydroxyl group interacts more closely with  $\text{Ti}^{3+}$  while elongating the C–O bond. The barrier to DDO over this reduced  $\text{TiO}_2/\text{Pd}$  interface is 0.41 eV, significantly lower relative to the Pd (1 1 1) surface (0.95 eV). The interfacial DDO reaction is nearly thermoneutral at 0.13 eV.

**TiO<sub>2-x</sub>/Pd Reduced Surface (O Vacancy):** Furfuryl alcohol adsorbs at the oxygen vacant  $\text{TiO}_2/\text{Pd}$  interface with the furyl ring

on the Pd surface and the hydroxyl group in the oxygen vacancy position (Fig. 6f). The adsorption energy is  $-2.66$  eV, stronger than adsorption to bare Pd (1 1 1) ( $-1.87$  eV). The barrier to break the C–O bond is just  $0.20$  eV, considerably lower than over bare Pd (1 1 1) ( $E_{act} = 0.95$  eV). Also, the step is highly exothermic over this site ( $-0.87$  eV) with OH filling the oxygen vacancy. The high exothermicity and considerably lower barrier for DDO suggest a synergistic role of multicomponent  $\text{TiO}_2/\text{Pd}$  system for significantly favoring C–O bond activation relative to Pd (1 1 1). Completing the reaction cycle to form the final hydrogenated products and re-form the vacancy is discussed in a later section.

We also examined DDO at the oxygen vacant interface with furfuryl alcohol oriented vertically to the surface (Fig. 6g). Although the vertical orientation is less favorable under the simulated conditions, prior work has suggested that vertical adsorption orientations may be important on crowded surfaces favored under reaction conditions [38]. The DDO barrier is also lowered in this orientation to  $0.51$  eV at the  $\text{TiO}_2/\text{Pd}$  interface versus  $1.19$  eV on bare Pd (1 1 1) (Fig. 5 label  $\text{TiO}_{2-x}/\text{Pd}$  (O vacancy), upright). This result suggests that the reduced  $\text{TiO}_2/\text{Pd}$  interface may promote DDO even if interfacial crowding prevents flat adsorption with the ring parallel to the surface.

The enhancement of DDO at a  $\text{TiO}_2/\text{Pd}$  interface is not unique to our  $\text{TiO}_2$  nanowire model. A second  $\text{TiO}_2/\text{Pd}$  interfacial model was developed to provide qualitative comparison with this nanowire model and check the robustness of mechanistic conclusions. A finite 6-atom  $\text{Ti}_2\text{O}_4$  cluster, adsorbed to a Pd (1 1 1) surface (Figure S1a), also showed a low C–O bond activation barrier of  $0.27$  eV with the reaction being highly exergonic (Figure S1b). This indicates that the synergistic role of  $\text{TiO}_2/\text{Pd}$  interface in promoting deoxygenation of furfuryl alcohol is not highly sensitive to model assumptions about the interfacial structure (see SI for further details). Also, the strain-free nature of the second model validates our assumption that the  $8.3\%$  strain in the developed nanowire model does not alter our conclusions, but only the absolute energy values.

**3.2.1.3. Inert pore model.** The DDO barrier was also studied over the inert helium pore model with a pore diameter of  $7$  Å. The pore imposes a steric effect causing furfuryl alcohol to adsorb in an

upright conformation with the furyl ring away from the metal surface and only the hydroxyl group bound to the surface (B.E. =  $-0.65$  eV vs  $-1.87$  eV on bare Pd, see Fig. 6h). Similar to upright adsorption over the bare Pd (1 1 1) surface (Fig. 5), the barrier is high at  $1.30$  eV. Thus, crowding to orient adsorbates vertically, despite causing direct surface-OH interaction, does not accelerate DDO. The chemical functionality of reduced  $\text{TiO}_2$  sites at the interface is needed to accelerate C–O activation, rather than solely steric control of furfuryl alcohol orientation.

### 3.2.2. Hydrodeoxygenation (HDO) – H-assisted deoxygenation

The HDO pathway assists C–O breaking via concerted H–OH bond formation thereby activating the C–O bond with water formation:  $\text{C}_4\text{H}_3\text{O}(\text{CH}_2\text{OH})^* + \text{H}^* \rightarrow \text{C}_4\text{H}_3\text{O}(\text{CH}_2)^* + \text{H}_2\text{O}^*$ . The hydrodeoxygenation of furfuryl alcohol to 2-methylfuran then completes with subsequent methyl hydrogenation. Potential energy surfaces (PES) of HDO paths across different DFT models are shown in Fig. 7.

**3.2.2.1. Bare Pd (1 1 1).** Prior to the HDO step, both hydrogen and furfuryl alcohol are co-adsorbed over neighbouring hollow sites. The C–O activation proceeds in an unconcerted fashion with two steps: a) H attaching to the hydroxyl group forming the H–OH bond ( $E_{act} = 0.85$  eV) (Fig. 8a) and then b) the subsequent C–O breaking to give away a water molecule and a  $\text{C}_4\text{H}_3\text{O}(\text{CH}_2)^*$  intermediate (Fig. 8b) with the overall barrier being  $1.15$  eV. Thus, direct deoxygenation has a lower barrier than this H-assisted deoxygenation on Pd (1 1 1). A similar barrier of  $0.85$  eV has been reported for H addition to the hydroxyl group over bare Pd (1 1 1) by Vorotnikov et al. [29] with their transition state structure appearing equivalent to ours for the first step in this process. However, they did not locate the subsequent higher energy transition state that needs to be overcome for C–O bond dissociation.

**3.2.2.2. Rutile- $\text{TiO}_2$  nanowire over Pd (1 1 1) surface.** We explored the HDO mechanism starting at a stoichiometric interface with hydrogen and furfuryl alcohol co-adsorbed over neighboring hollow sites on the Pd surface at the interface. During hydrodeoxygenation at this interface, the C–O bond is activated after the hydrogen attaches to the hydroxyl group of furfuryl alcohol

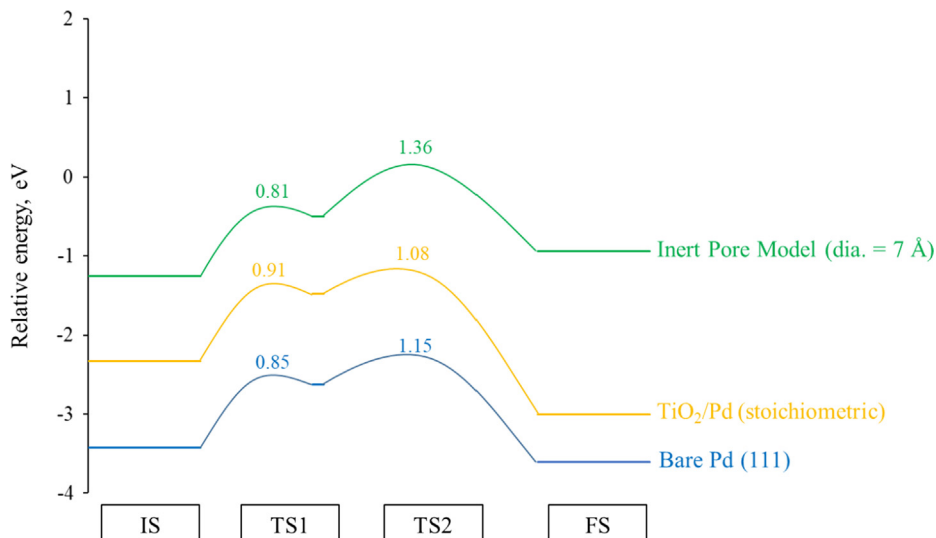


**Fig. 7.** Potential energy surfaces (PES) of HDO paths over different DFT models. Initial and final state energies are plotted with respect to the energy of gas phase furfuryl alcohol,  $1/2 \text{H}_2$  and the respective surface models without hydrocarbons adsorbed. Activation energy barriers ( $E_a$ ) in electronvolts are labelled relative to the initial states. The intermediate structures between the two transition states were approximately of the same energy as the first transition structure. The transition state structures are illustrated in Fig. 8.

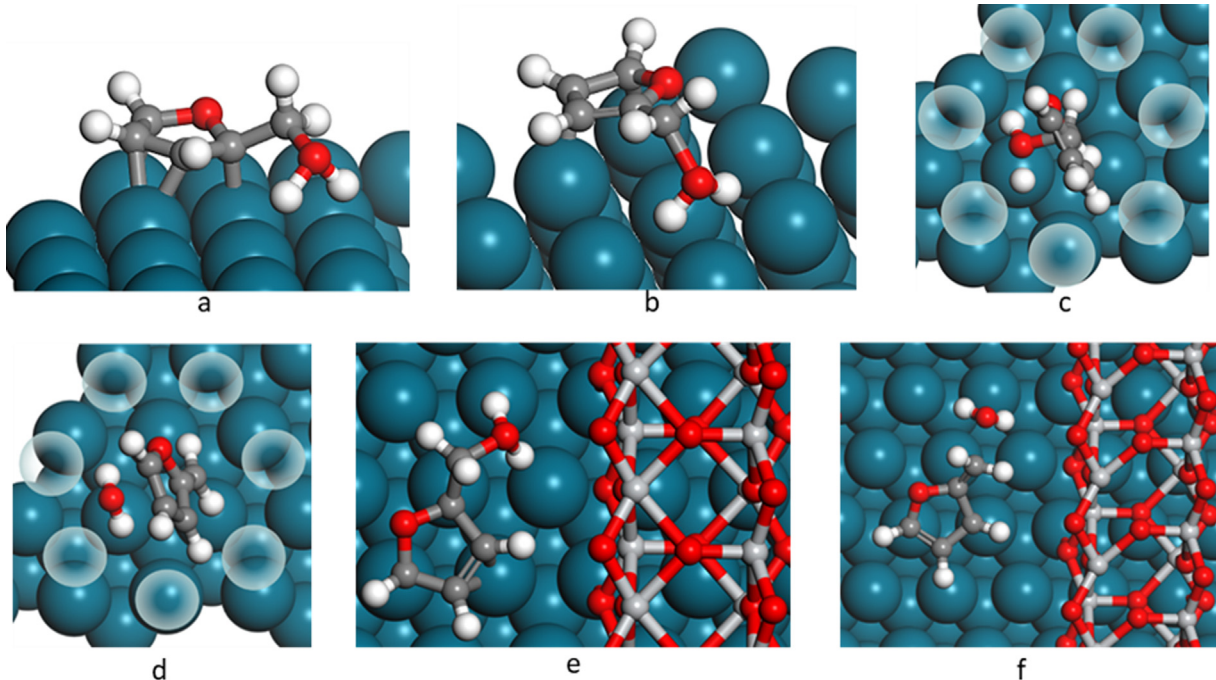


**Fig. 8.** Transition states for HDO across different models: (a) bare Pd (1 1 1) with hydrogen from the surface attaching to the hydroxyl group, (b) bare Pd (1 1 1) with C=O activation via  $\text{H}_2\text{O}$  formation, (c) inert pore model (pore diameter = 7 Å) with H attaching to hydroxyl group and forming H-OH bond, (d) inert pore model (pore diameter = 7 Å) with C=O activation via  $\text{H}_2\text{O}$  formation (helium pore atoms are shown transparent for clarity), (e)  $\text{TiO}_2/\text{Pd}$  stoichiometric interface with H-OH formation and (f)  $\text{TiO}_2/\text{Pd}$  stoichiometric interface with C=O activation via removal of  $\text{H}_2\text{O}$ . Initial and final states' structures across these DFT models are tabulated in Table S3.

(Fig. 8e). This entity finally dissociates to produce a water molecule (Fig. 8f) which is adsorbed over the oxide interface. The overall HDO barrier (1.08 eV) is similar to that without the interface on Pd (1 1 1) ( $E_{\text{act}} = 1.15$  eV). The mechanism was also probed at a reduced interface,  $\text{TiO}_{2-x}/\text{Pd}$  with hydrogen adsorbed on an O atom of  $\text{TiO}_2$ . However, hydrogen spilled over to the Pd surface at the interface during this transition state search such that both searches led to effectively the same transition state. HDO at an oxygen deficient interface,  $\text{TiO}_{2-x}/\text{Pd-H}$ , was not considered since the C=O bond of furfuryl alcohol is activated so easily at this site through DDO ( $E_{\text{act}} = 0.20$  eV). Thus, the interfacial sites are unable to accelerate deoxygenation through HDO and direct deoxygenation should be the most feasible path at the  $\text{TiO}_2/\text{Pd}$  interface.

**3.2.2.3. Inert pore model.** We examined whether the inert pore model would promote HDO by forcing furfuryl alcohol and subsequent intermediates to orient vertically along the surface normal. The degree of steric constraints was varied by changing the pore

diameter. During HDO, the molecular fragments are weakly adsorbed upright over the available Pd sites within the pore (Fig. 8c and d). As reported in Fig. 9a, with decrease in pore size (increase in steric crowding), the HDO activation barrier is not significantly affected relative to that on bare Pd. The H-assisted deoxygenation mechanism is negligibly affected upon change in adsorption conformations due to steric effects.

### 3.2.3. Decarbonylation

As reported by Vorotnikov et al. [29], the preferred paths for furfuryl alcohol decarbonylation to furan go through an acyl intermediate  $\text{C}_4\text{H}_3\text{O}(\text{CO})^*$ . C=C cleavage of this intermediate leads to co-adsorbed furyl ( $\text{C}_4\text{H}_3\text{O}^*$ ) and  $\text{CO}^*$ . Furyl hydrogenation produces furan. The C=C cleavage is the key step in decarbonylation, and we consider only this step as an indicator of selectivity to furan. We compute the reaction energies and barriers for the C=C cleavage step on Pd (1 1 1),  $\text{TiO}_2/\text{Pd}$  interfaces, and under steric constraints via the inert pore model. Potential energy surfaces (PES)

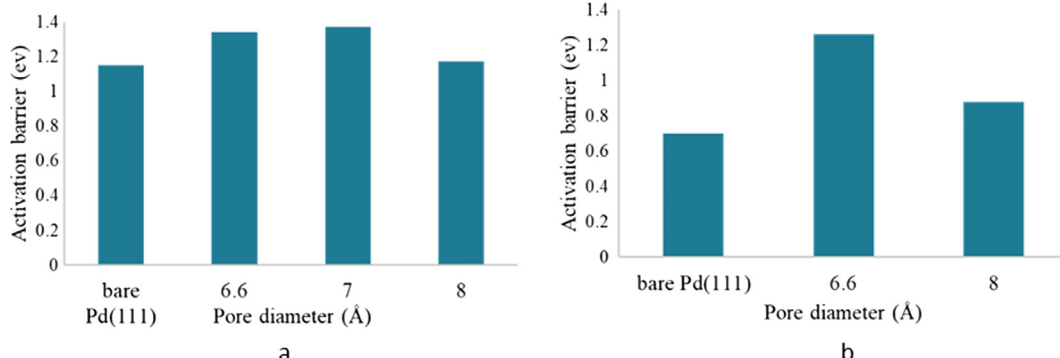


**Fig. 9.** (a) Hydrodeoxygenation barrier over the inert pore model for different pore diameters compared with that on bare Pd (1 1 1), (b) Decarbonylation barrier over the inert pore model for different pore diameters relative to bare Pd (1 1 1).

of DCO path across different DFT models are shown and compared in Fig. 10.

**3.2.3.1. Bare Pd (1 1 1).** Over bare Pd, the acyl intermediate ( $C_4H_3O(CO)^*$ ) adsorbs over a fcc hollow site with the C—CO bond directly atop a Pd atom (Fig. 11a). C—C bond cleavage has a barrier of 0.71 eV and the reaction is exothermic by 0.52 eV (Fig. 10). These energetics agree well with the DFT results reported by Vorotnikov et al. [29].

**3.2.3.2. Rutile- $TiO_2$  nanowire over Pd (1 1 1) surface.** We examined the role of interfacial sites in activating the C—C bond of the acyl intermediate ( $C_4H_3O(CO)^*$ ) over stoichiometric, reduced and oxygen deficient interfacial sites. We probed various adsorption sites for the acyl intermediate, furyl and CO species (see Fig. 11b, c and d) at these interfacial sites, however, we found no indication that the oxide/metal interface activates the C—C bond faster or more favorably than the pure Pd (1 1 1) surface.

Adsorption of both reactants (acyl intermediate) and products (furyl, CO) is generally stronger at the  $TiO_2$ /Pd interface. Adsorption is promoted through electron transfer from the nanowire to Pd and H-bonding interactions with  $TiO_2$ . Adsorption is strengthened relatively equally for the reactants and the products such that the decarbonylation reaction does not become more favorable at the interface.

The C—C cleavage barrier is slightly raised over each type of interfacial site and the reaction is similarly exergonic to that on Pd (1 1 1). Over the reduced interface, the barrier of 0.70 eV is comparable to bare Pd. Over the stoichiometric interface, the barrier increases to 0.91 eV. The barrier over an oxygen deficient site increases to 0.93 eV. Though the interface is able to stabilize some adsorbed states, the chemical functionality offered by the interface does not offer any significantly enhanced transition state stabilization for decarbonylation. In short, the presence of interfacial sites does not accelerate the reaction kinetics for DCO as it does for DDO. This implies an increased selectivity towards deoxygenation over interfacial sites.

**3.2.3.3. Inert pore model.** Kumar et al. [20] previously reported that self-assembled monolayers on Pd could increase selectivity to 2-methylfuran by slowing decarbonylation. This occurred by preventing flat adsorption of the furyl ring. We, therefore, explored whether steric constraints could slow decarbonylation. Using the inert pore model, we examined the effect of steric constraints on the C—C activation of the acyl intermediate. The barriers for the C—C bond breaking step for the pore diameters 6.6 Å and 8 Å are given in Fig. 9b. For the pore diameter of 6.6 Å, the acyl intermediate  $C_4H_3O(CO)^*$  adsorbs in an upright geometry (Fig. 11e). For the pore diameter of 8 Å, the acyl species adsorbs in a tilted geometry intermediate between flat and upright adsorption (Fig. 11f). With upright adsorption in the 6.6 Å pore, both carbons across the dissociating C—CO bond cannot interact with the Pd surface and thus a significantly higher energy barrier (~1.26 eV) is calculated relative to flat adsorption over Pd (1 1 1) (Fig. 9b). The 8 Å pore leads to an energy barrier (0.88 eV) in between that of the 6.6 Å pore and that of the pure Pd (1 1 1) (0.71 eV). Transition state structures are illustrated in Table S4.

These results suggest that surface crowding, possibly induced by significant coverage on the Pd surface by  $TiO_2$ , could increase selectivity to 2-methylfuran by raising the decarbonylation barriers. However, if this was the sole effect of  $TiO_2$  encapsulation, 2-methylfuran production would also be slowed due to the blocking of much of the surface. The substantial decrease in DDO barrier at the reduced  $TiO_2$ /Pd interface offers enhanced 2-methylfuran production rates while possibly also slowing decarbonylation by limiting room for flat adsorption.

### 3.3. Complete reaction scheme for direct deoxygenation

In the previous section, we explored the key steps that differentiated DDO, HDO and DCO mechanisms. Since the elementary DDO step was accelerated over the oxygen deficient and reduced interfaces, we now consider the reaction energetics for the full DDO catalytic cycle over the reduced interface  $TiO_{2-x}$ /Pd-H and the oxygen deficient interface  $TiO_{2-x}$ /Pd. The results presented in this section

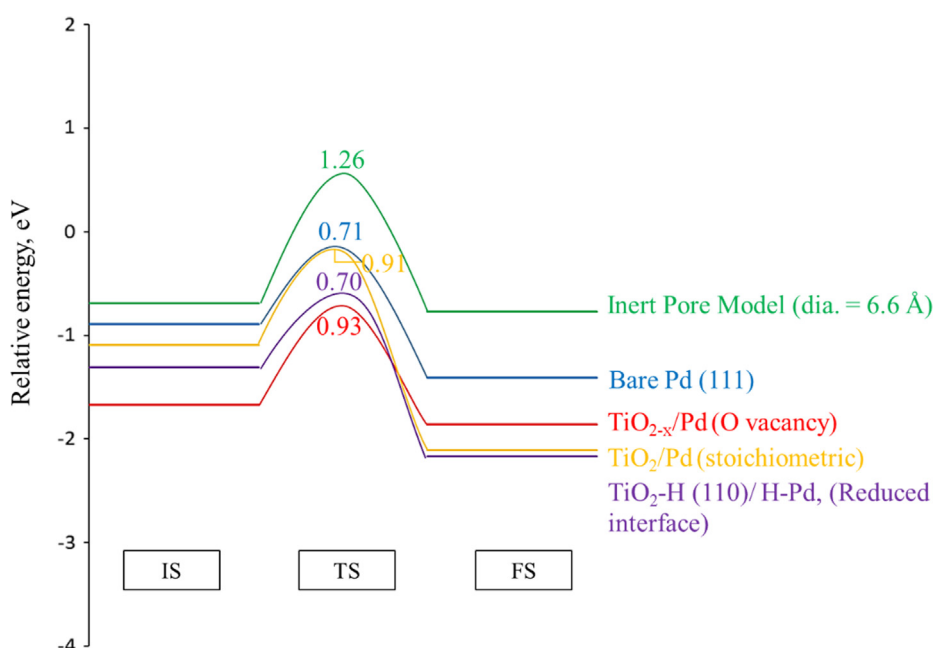


**Fig. 10.** Potential energy surfaces (PES) of DCO path over different DFT models. Initial and final state energies are plotted with respect to the energy of gas phase furfural minus 1/2  $H_2$  and the respective surface models without hydrocarbons adsorbed. Activation energy barriers ( $E_a$ ) in electronvolts are labelled. Transition state structures are illustrated in Fig. 11.

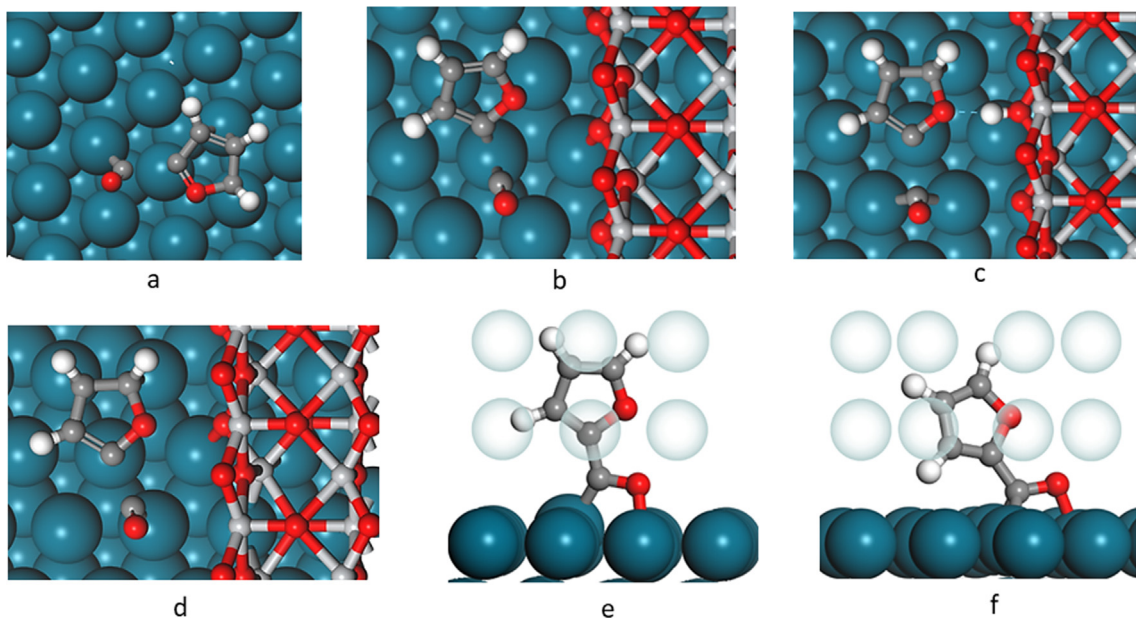


**Fig. 11.** Transition states for decarbonylation across different models: (a) bare Pd (1 1 1), (b) TiO<sub>2</sub>/Pd stoichiometric interface, (c) TiO<sub>2</sub>-H/Pd reduced interface and (d) TiO<sub>2-x</sub>/Pd oxygen deficient interface; adsorption of (e) acyl intermediate with upright conformation and no C—C activation over the inert pore model (diameter = 6.6 Å) and (f) acyl intermediate with slight C—C activation over the inert pore model (diameter = 8 Å). Helium pore atoms are shown transparent in e and f for clarity. Initial and final states' structures (and TS states over the inert pore model) across these DFT models are tabulated in Table S4.

demonstrate that the lowered DDO barrier will result in an enhanced overall 2-methylfuran formation rate at the reduced interface.

### 3.3.1. DDO mechanism: over reduced interface (TiO<sub>2</sub>-H (1 1 0)/Pd-H)

The DDO reaction sequence over a reduced interface begins with the adsorption of hydrogen and furfuryl alcohol. The alcohol adsorbs over a hollow site on the Pd surface such that its hydroxyl group forms a Ti—OH bond with the reduced Ti<sup>3+</sup> atom (Fig. 12, state a). The DDO step proceeds over a barrier of 0.41 eV.

After deoxygenation, the intermediate 2-methylfuryl species C<sub>4</sub>H<sub>3</sub>O(CH<sub>2</sub>)<sup>+</sup> adsorbs over the Pd hcp-hollow site whereas the hydroxyl OH<sup>−</sup> adsorbs directly to the interfacial Ti<sup>3+</sup> site. To obtain the final product 2-methylfuran, H from TiO<sub>2</sub> or from the Pd surface can be added to the methyl carbon. These barriers (0.17 eV, Table S1 step IXb) are similar due to thermoneutral H spillover between Pd and O of TiO<sub>2</sub> near the co-adsorbed 2-methylfuryl species at the interface. To complete the reaction sequence, the Ti<sup>4+</sup>OH<sup>−</sup> species is reduced to a water molecule by the hydrogen adsorbed on the Pd (state b, Fig. 12). The barrier for this step is as low as 0.17 eV (depending on initial H adsorption site) with reaction energy downhill by 0.27 eV (Table S1, step XIIIc). The final 2-methylfuran and water desorption costs are 1.86 eV and 1.11 eV, respectively. With H adsorption over TiO<sub>2</sub> ( $E_{\text{ads}} = -0.3$  eV) through spillover from Pd, the catalytic cycle is regenerated to form the reduced interface H-TiO<sub>2</sub>/Pd. Desorption would be promoted by higher adsorbate coverages and more favorable if entropy was considered.

### 3.3.2. DDO Mechanism: TiO<sub>2-x</sub>/Pd reduced surface (oxygen deficient)

Since the C—O dissociation step is accelerated over the TiO<sub>2-x</sub>/Pd oxygen deficient surface, we examine the complete catalytic cycle for furfuryl alcohol deoxygenation to 2-methylfuran. Adsorption of furfuryl alcohol occurs near a vacant site, such that the OH group interacts with the vacancy (state a, Fig. 13). The furan ring of the molecule is adsorbed over a hcp-hollow site. To break the C—OH bond, the barrier is only 0.20 eV and the reaction is highly exothermic by 0.87 eV, as discussed earlier. The hydroxyl OH<sup>−</sup> adsorbs and

occupies the vacant oxygen site whereas the intermediate fragment 2-methylfuryl C<sub>4</sub>H<sub>3</sub>O(CH<sub>2</sub>)<sup>+</sup> is adsorbed over the Pd fcc-hollow site (state b, Fig. 13). Next, hydrogen from the interface is transferred to the methyl group over a small barrier of 0.17 eV to give 2-methylfuran (state c, Fig. 13). This hydrogenation step at the interface is easier than on bare Pd (1 1 1) where the barrier is 0.62 eV. To close the catalytic cycle, there is an energetic cost to regenerate the vacancy. As discussed earlier, the cost for creating an oxygen vacancy is limited by the thermodynamic reaction energy of 0.81 eV (on the hydrogenated TiO<sub>2</sub> interface without H<sub>2</sub>O co-adsorbed) or an activation barrier of 0.40 eV when stabilized by a co-adsorbed H<sub>2</sub>O. The reaction schematic diagram in Fig. 13 includes the latter precursor state for water desorption to illustrate a realistic reaction environment. Finally, as also examined earlier, it costs 1.11 eV for subsequent water desorption relative to this state (Table S1, step Xb). Additionally, it costs 1.86 eV to desorb the 2-methylfuran adsorbed at this interface. The product desorption and water desorption energies are higher than the activation barriers in this reaction scheme. However, these energies do not include the entropy gained through the formation of gas phase species. Furthermore, these desorption energies would be coverage dependent. Thus, under surface crowding with furfuryl oxygenates and other co-adsorbates, these desorption energies could become more favorable. For example, in the presence of a second 2-methylfuran adsorbed at the interface, the desorption energy for the first 2-methylfuran decreases significantly from 1.86 eV to 0.72 eV.

The reaction schematic in Fig. 13 also includes the activation barriers over Pd (1 1 1). On comparison, the DDO catalytic cycle over an oxygen deficient TiO<sub>2-x</sub>/Pd interface will be more favorable than over Pd (1 1 1) due to relatively lower barriers and exothermic reaction steps, and emphasizes the role of oxygen vacancies in the deoxygenation chemistry hypothesized earlier.

Overall, we conclude that in the presence of reduced Ti<sup>3+</sup> sites and oxygen vacancies, the dissociation of the C—OH bond (direct deoxygenation) is thermodynamically as well as kinetically far more feasible than that observed over the Pd (1 1 1) surface. Regeneration of these reduced active sites is also energetically feasible, completing the catalytic cycle.

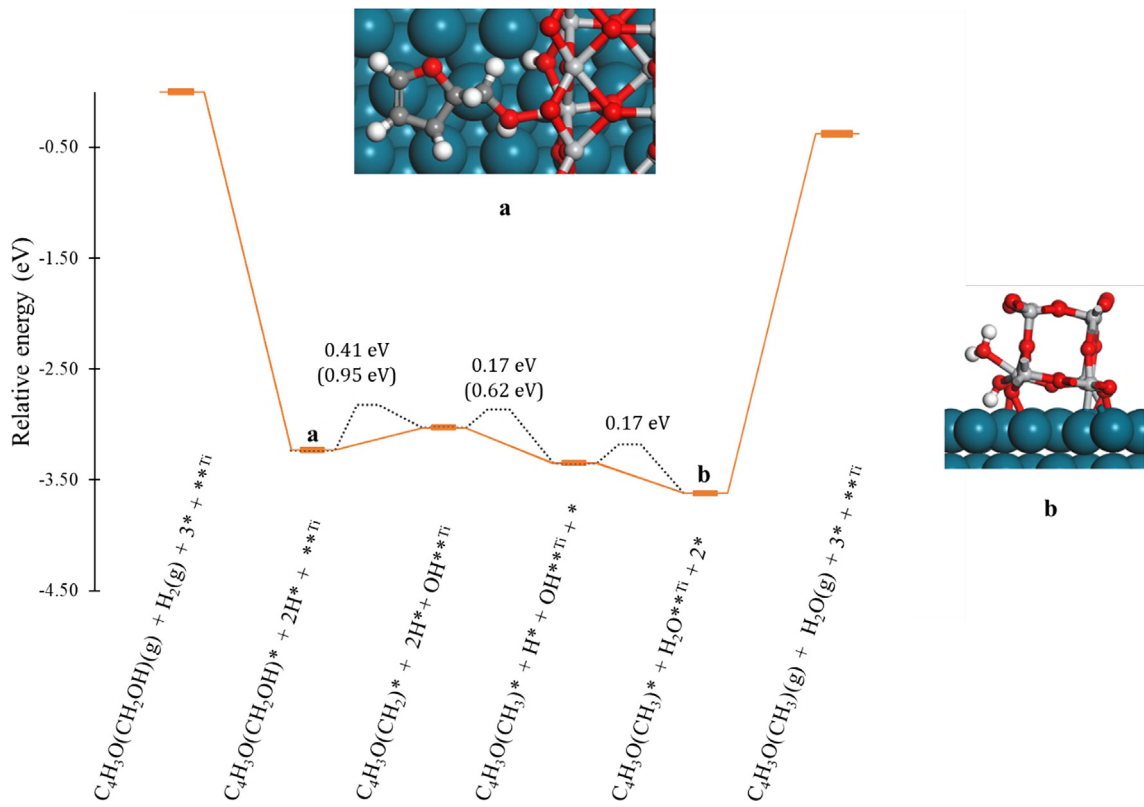


**Fig. 12.** Reaction energy diagram for DDO of furfuryl alcohol over a TiO<sub>2</sub>-H/Pd-H reduced interface. The values in parentheses are the activation energies for corresponding steps over bare Pd (1 1 1). \* and \*\*<sub>Ti</sub> refer to Pd sites and Ti sites of TiO<sub>2</sub> at the interface, respectively.

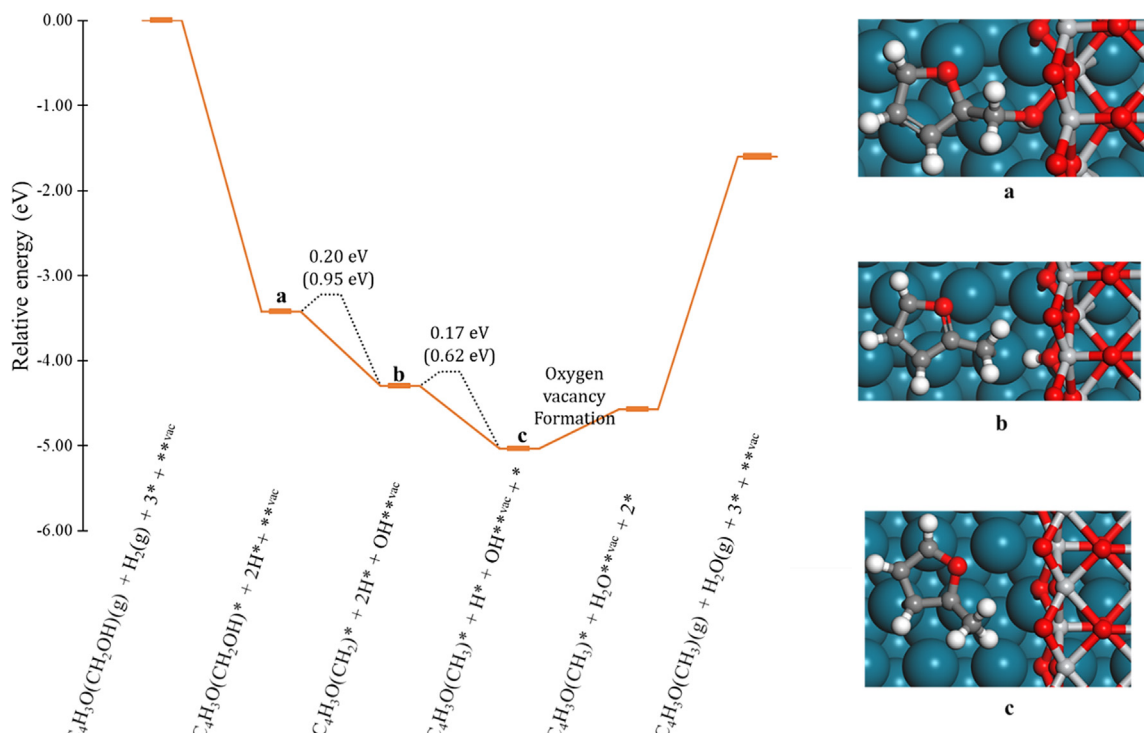


**Fig. 13.** Reaction energy diagram for DDO of furfuryl alcohol at a TiO<sub>2-x</sub>/Pd reduced surface (oxygen deficient). The values in parentheses are the activation energies for corresponding steps over bare Pd (1 1 1). \* and \*\*<sub>vac</sub> refer to Pd sites and TiO<sub>2</sub> vacancy sites at the interface, respectively.

### 3.4. DDO vs DCO selectivity

Over reduced interfacial sites, lowered DDO barriers were observed, whereas DCO had higher barriers at the interface and under interfacial crowding. Analysing activity and selectivity on a simplified semi-quantitative basis, the enhanced activity (per site) to DDO caused by interfacial sites can be approximated through the relative activation barriers:

$$\frac{k_{DDO,interface}}{k_{DDO,barePd}} \approx \exp\left(\frac{E_a^{bare,Pd} - E_a^{interface}}{RT}\right) \approx \exp\left(\frac{0.95 - 0.20}{RT}\right)$$

$$\approx 6.98 \times 10^8$$

where similar pre-exponential factors have been assumed for the two rate expressions over the interface and bare Pd (1 1 1). We have only considered the activation barriers for C—OH deoxygenation steps over the two surfaces for simplicity (temperature = 443 K [12]), which compares the rate constant for the DDO step between reduced interfacial sites and non-TiO<sub>2</sub> coated Pd sites. To compare practical rates, we would also need to multiply this value by the relative density of active sites and the relative coverage of adsorbed intermediates. The number of Pd sites on a non-TiO<sub>2</sub> coated Pd nanoparticle could be much larger compared to the number of reduced TiO<sub>2</sub>/Pd interfacial sites on a coated Pd particle, and this site ratio is difficult to quantify. Also, the effective coverage of species would be different on both types of catalytic systems due to differences in the adsorption energy of furfuryl alcohol. However, the  $\sim 10^8$  ratio of per-site rate constants suggests that, even if TiO<sub>2</sub> encapsulation blocks a vast majority of Pd sites, the few reduced interfacial sites would give a significant enhancement in DDO activity relative to pure Pd.

Considering a similar simplified kinetic analysis, selectivity to deoxygenation towards 2-methylfuran over decarbonylation ( $\approx k_{DDO}/k_{DCO}$ ) is  $\sim 7.9 \times 10^5$  over the reduced TiO<sub>2</sub>/Pd interface, whereas this selectivity is of the order  $\sim 10^{-3}$  over the bare Pd (1 1 1) surface. A complete microkinetic model that incorporates all the elementary steps and also addresses relative site populations, could more precisely illustrate this activity and selectivity, however, the simplified analysis suggests that the lowered barrier over interfacial sites can completely alter selectivity towards 2-methylfuran while not reducing the rate of 2-methylfuran production. This is consistent with the experimental results for furfuryl alcohol deoxygenation over Pd-TiO<sub>2</sub> core-shell catalysts where a sizable increase in selectivity to 2-methylfuran has been reported relative to non-encapsulated Pd particles [12]. Also, selectivity of the order of  $10^{-3}$  over Pd (1 1 1) is consistent with the experiments over supported Pd catalysts in which most of the furfuryl alcohol converts to furan [10].

Lastly, though on a more qualitative basis, upright adsorption over the inert pore model (pore diameter of 6.6 Å) causes significant increase in the energy barrier for C—C activation (~1.26 eV). DDO still occurs with favorable energetics with upright adsorption at the oxygen deficient interface. Thus, deoxygenation would be favored if small TiO<sub>2</sub> pores produced sterically constrained interfacial sites. This is consistent with the numerous experimental studies employing surface modifiers to improve selectivity by effectively blocking decarbonylation over other reaction steps [39] and thus supports that orientation-induced selectivity may also contribute to promoting deoxygenation over decarbonylation.

## 4. Conclusion

We considered the adsorption and reaction of furfuryl alcohol near interfacial sites composed of a Pd (1 1 1) surface and an adsorbed rutile TiO<sub>2</sub> nanowire. This was contrasted with reaction

over the Pd (1 1 1) surface. The role of metal oxide/metal interface towards promoting deoxygenation was considered over different interfacial sites: (i) the TiO<sub>2</sub>/Pd interface reduced by hydrogen adsorption and formation of Ti<sup>3+</sup> ions and (ii) an oxygen deficient interface with a vacancy created by H<sub>2</sub>O desorption from the hydroxylated TiO<sub>2</sub>/Pd interface. DFT results show that these reduced interfacial sites lower the barriers for C—OH cleavage significantly. Additionally, the interface does not promote activation of the C—C bond, therefore promoting DDO over DCO. Combining the results over the selective DDO and non-selective DCO paths and the simplified kinetic analysis, a sizable rise in selectivity towards 2-methylfuran, the desired product, is explained for TiO<sub>2</sub> encapsulated Pd catalysts. Isotopic labelling for studying oxygen exchange of these oxygenated adsorbates with TiO<sub>2</sub> may prove beneficial in asserting the role of the reducible oxides' interface experimentally.

## Acknowledgements

The authors acknowledge support from the National Science Foundation for funding this research through DMREF Grant #1436206. This work used the Extreme Science and Engineering Discovery Environment (XSEDE), which is supported by National Science Foundation grant number ACI-1053575. S. Deo acknowledges training provided by the Computational Materials Education and Training (CoMET) NSF Research Traineeship (grant number DGE-1449785).

## Appendix A. Supplementary material

Supplementary data to this article can be found online at <https://doi.org/10.1016/j.jcat.2019.07.012>.

## References

- [1] K. Xiong, W.M. Wan, J.G.G. Chen, Reaction pathways of furfural, furfuryl alcohol and 2-methylfuran on Cu(111) and NiCu bimetallic surfaces, *Surf. Sci.* 652 (2016) 91–97.
- [2] K. Gupta, R.K. Rai, S.K. Singh, Metal catalysts for the efficient transformation of biomass-derived HMF and furfural to value added chemicals, *ChemCatChem* 10 (2018) 2326–2349.
- [3] A. Banerjee, S.H. Mushrif, Investigating reaction mechanisms for furfural hydrodeoxygenation on Ni and the effect of boron doping on the activity and selectivity of the catalyst, *J. Phys. Chem. C* 122 (2018) 18383–18394.
- [4] N.M. Briggs, L. Barrett, E.C. Wegener, L.V. Herrera, L.A. Gomez, J.T. Miller, S.P. Crossley, Identification of active sites on supported metal catalysts with carbon nanotube hydrogen highways, *Nat. Commun.* 9 (2018) 3827.
- [5] M.J. Gilkey, P. Panagiotopoulou, A.V. Mironenko, G.R. Jennings, D.G. Vlachos, B.J. Xu, Mechanistic insights into metal Lewis acid-mediated catalytic transfer hydrogenation of furfural to 2-methylfuran, *ACS Catal.* 5 (2015) 3988–3994.
- [6] C. Newman, X.B. Zhou, B. Goundie, I.T. Ghompson, R.A. Pollock, Z. Ross, M.C. Wheeler, R.W. Meulenberg, R.N. Austin, B.G. Frederick, Effects of support identity and metal dispersion in supported ruthenium hydrodeoxygenation catalysts, *Appl. Catal. A Gen.* 477 (2014) 64–74.
- [7] M.J. Taylor, L. Jiang, J. Reichert, A.C. Papageorgiou, S.K. Beaumont, K. Wilson, A.F. Lee, J.V. Barth, G. Kyriakou, Catalytic hydrogenation and hydrodeoxygenation of furfural over Pt(111): a model system for the rational design and operation of practical biomass conversion catalysts, *J. Phys. Chem. C* 121 (2017) 8490–8497.
- [8] S.K. Jaatinen, R.S. Karinen, J.S. Lehtonen, Liquid phase furfural hydrotreatment to 2-methylfuran with carbon supported copper, nickel, and iron catalysts, *ChemistrySelect* 2 (2017) 51–60.
- [9] S. Sitthisa, D.E. Resasco, Hydrodeoxygenation of furfural over supported metal catalysts: a comparative study of Cu, Pd and Ni, *Catal. Lett.* 141 (2011) 784–791.
- [10] S.H. Pang, J.W. Medlin, Adsorption and reaction of furfural and furfuryl alcohol on Pd(111): unique reaction pathways for multifunctional reagents, *ACS Catal.* 1 (2011) 1272–1283.
- [11] G. Li, Z. Tang, Noble metal nanoparticle@metal oxide core/yolk-shell nanostructures as catalysts: recent progress and perspective, *Nanoscale* 6 (2014) 3995–4011.
- [12] J. Zhang, B. Wang, E. Nikolla, J.W. Medlin, Directing reaction pathways through controlled reactant binding at Pd-TiO<sub>2</sub> interfaces, *Angew. Chem.* 129 (2017) 6694–6698.

- [13] T.O. Omotoso, B. Baek, L.C. Grabow, S.P. Crossley, Experimental and first-principles evidence for interfacial activity of Ru/TiO<sub>2</sub> for the direct conversion of m-cresol to toluene, *ChemCatChem* 9 (2017) 2642–2651.
- [14] H.Y.T. Chen, G. Pacchioni, Role of oxide reducibility in the deoxygenation of phenol on ruthenium clusters supported on the anatase titania (1 0 1) surface, *ChemCatChem* 8 (2016) 2492–2499.
- [15] O.F. Aldosari, S. Iqbal, P.J. Miedziak, G.L. Brett, D.R. Jones, X. Liu, J.K. Edwards, D.J. Morgan, D.K. Knight, G.J. Hutchings, Pd-Ru/TiO<sub>2</sub> catalyst - an active and selective catalyst for furfural hydrogenation, *Catal. Sci. Technol.* 6 (2016) 234–242.
- [16] G.M. King, S. Iqbal, P.J. Miedziak, G.L. Brett, S.A. Kondrat, B.R. Yeo, X. Liu, J.K. Edwards, D.J. Morgan, D.K. Knight, G.J. Hutchings, An investigation of the effect of the addition of tin to 5 %Pd/TiO<sub>2</sub> for the hydrogenation of furfuryl alcohol, *ChemCatChem* 7 (2015) 2122–2129.
- [17] P.M. de Souza, L. Nie, L.E.P. Borges, F.B. Noronha, D.E. Resasco, Role of oxophilic supports in the selective hydrodeoxygenation of m-cresol on Pd catalysts, *Catal. Lett.* 144 (2014) 2005–2011.
- [18] M. Lu, H. Du, B. Wei, J. Zhu, M. Li, Y. Shan, C. Song, Catalytic Hydrodeoxygenation of guaiacol over palladium catalyst on different titania supports, *Energy Fuels* 31 (2017) 10858–10865.
- [19] R.C. Nelson, B. Baek, P. Ruiz, B. Goundie, A. Brooks, M.C. Wheeler, B.G. Frederick, L.C. Grabow, R.N. Austin, Experimental and Theoretical insights into the hydrogen-efficient direct hydrodeoxygenation mechanism of phenol over Ru/TiO<sub>2</sub>, *ACS Catal.* 5 (2015) 6509–6523.
- [20] G. Kumar, C.-H. Lien, M.J. Janik, J.W. Medlin, catalyst site selection via control over noncovalent interactions in self-assembled monolayers, *ACS Catal.* 6 (2016) 5086–5094.
- [21] J.P. Perdew, Y. Wang, Accurate and simple analytic representation of the electron-gas correlation energy, *Phys. Rev. B* 45 (1992) 13244–13249.
- [22] S. Grimme, J. Antony, S. Ehrlich, H. Krieg, A consistent and accurate ab initio parametrization of density functional dispersion correction (DFT-D) for the 94 elements H-Pu, *J. Chem. Phys.* 132 (2010) 154104.
- [23] P.E. Blöchl, Projector augmented-wave method, *Phys. Rev. B* 50 (1994) 17953–17979.
- [24] A consistent and accurate ab initio parametrization of density functional dispersion correction (DFT-D) for the 94 elements H-Pu, *J. Chem. Phys.* 132 (2010) 154104.
- [25] Z. Hu, H. Metiu, Choice of U for DFT+U calculations for titanium oxides, *J. Phys. Chem. C* 115 (2011) 5841–5845.
- [26] H.J. Monkhorst, J.D. Pack, Special points for Brillouin-zone integrations, *Phys. Rev. B* 13 (1976) 5188–5192.
- [27] Nudged-elastic band used to find reaction coordinates based on the free energy, *J. Chem. Phys.* 140 (2014) 074109.
- [28] A dimer method for finding saddle points on high dimensional potential surfaces using only first derivatives, *J. Chem. Phys.* 111 (1999) 7010–7022.
- [29] V. Vorotnikov, G. Mpourmpakis, D.G. Vlachos, DFT study of furfural conversion to furan, furfuryl alcohol, and 2-methylfuran on Pd(111), *ACS Catal.* 2 (2012) 2496–2504.
- [30] M. Vandichel, A. Moscu, H. Grönbeck, Catalysis at the rim: a mechanism for low temperature CO oxidation over Pt3Sn, *ACS Catal.* (2017) 7431–7441.
- [31] M. Ramamoorthy, D. Vanderbilt, R.D. King-Smith, First-principles calculations of the energetics of stoichiometric TiO<sub>2</sub>surfaces, *Phys. Rev. B* 49 (1994) 16721–16727.
- [32] H. Li, Y. Guo, J. Robertson, Calculation of TiO<sub>2</sub> surface and subsurface oxygen vacancy by the screened exchange functional, *J. Phys. Chem. C* 119 (2015) 18160–18166.
- [33] A. Ruiz Puigdollers, P. Schlexer, S. Tosoni, G. Pacchioni, Increasing oxide reducibility: the role of metal/oxide interfaces in the formation of oxygen vacancies, *ACS Catal.* 7 (2017) 6493–6513.
- [34] D.A. Gomez-Gualdrón, S.T. Dix, R.B. Getman, R.Q. Snurr, A modelling approach for MOF-encapsulated metal catalysts and application to n-butane oxidation, *Phys. Chem. Chem. Phys.* 17 (2015) 27596–27608.
- [35] W. Dong, J. Hafner, H<sub>2</sub> dissociative adsorption on Pd(111), *Phys. Rev. B* 56 (1997) 15396–15403.
- [36] H.L. Tierney, A.E. Baber, J.R. Kitchin, E.C.H. Sykes, Hydrogen dissociation and spillover on individual isolated palladium atoms, *Phys. Rev. Lett.* 103 (2009) 246102.
- [37] P.M. Kowalski, B. Meyer, D. Marx, Composition, structure, and stability of the rutile TiO<sub>2</sub>(110) surface: oxygen depletion, hydroxylation, hydrogen migration, and water adsorption, *Phys. Rev. B* 79 (2009) 115410.
- [38] S.H. Pang, A.M. Román, J.W. Medlin, Adsorption orientation-induced selectivity control of reactions of benzyl alcohol on Pd(111), *J. Phys. Chem. C* 116 (2012) 13654–13660.
- [39] C.A. Schoenbaum, D.K. Schwartz, J.W. Medlin, Controlling the surface environment of heterogeneous catalysts using self-assembled monolayers, *Acc. Chem. Res.* 47 (2014) 1438–1445.

Update

**Journal of Catalysis**

Volume 405, Issue , January 2022, Page 653–655

DOI: <https://doi.org/10.1016/j.jcat.2021.01.006>



## Corrigendum

Corrigendum to “Reaction paths for hydrodeoxygenation of furfuryl alcohol at TiO<sub>2</sub>/Pd interfaces” [J. Catal. 377 (2019) 28–40]Shyam Deo <sup>a</sup>, Will Medlin <sup>b</sup>, Eranda Nikolla <sup>c</sup>, Michael J. Janik <sup>a,\*</sup><sup>a</sup> Department of Chemical Engineering, The Pennsylvania State University, University Park, PA 16802, United States<sup>b</sup> Department of Chemical and Biological Engineering, University of Colorado Boulder, Boulder, CO 80303, United States<sup>c</sup> Department of Chemical Engineering and Materials Science, Wayne State University, Detroit, MI 48202, United States

The authors regret an error made in an input parameter in a density functional theory calculation that led some numbers in this publication to be erroneous.

In a paper recently published in Journal of Catalysis [1], we investigated the role of TiO<sub>2</sub> encapsulated Pd interfacial sites towards dictating hydrodeoxygenation (HDO) product selectivity for furfuryl alcohol using Density Functional Theory (DFT) calculations. A rutile TiO<sub>2</sub> (110) nanowire over a Pd (111) surface is used as the interfacial model. Interfacial TiO<sub>2</sub>/Pd sites were found to provide a bifunctional role that accelerated a direct-deoxygenation reaction path. TiO<sub>2</sub> generates reduced oxide sites that activate the C—O bond of furfuryl alcohol, with the alcohol group re-oxidizing the reduced site. The Pd surface activates H<sub>2</sub> and enables hydrogenation to the final product. Consequently, our results showed that deoxygenation is significantly accelerated over a TiO<sub>2-x</sub>/Pd oxygen deficient site, by a factor of ~10<sup>8</sup> at 443 K, altering the Pd selectivity from the undesired furan product to the desired 2-methylfuran.

Unfortunately, we found that the DFT input parameters used for calculating the energy of the oxygen deficient TiO<sub>2-x</sub>/Pd interface surface were inconsistent with the other reported DFT calculations. Consequently, adsorption energies or other energies relative to this surface were incorrectly reported in the paper. The major qualitative conclusions of the paper are not affected by this error. This errata corrects values in the text, figures, and Supplementary information that are impacted by the error. Also, all the corrected energetics reported in this paper are tabulated in the updated Supplementary Information, Table S1.

In section “2.3.2 Rutile-TiO<sub>2</sub> nanowire over the Pd (111) surface”, the oxygen vacancy formation energy reported for the interfacial oxygen atoms, in terms of the energy to desorb an oxygen atom as ½ O<sub>2</sub> as TiO<sub>2</sub> → TiO<sub>2-x</sub> + ½ O<sub>2</sub>, ranges between 3.11 and 3.18 eV, correcting the erroneous previously reported range of 3.67 and 3.74 eV. The updated range remains similar to that for the extended 3 × 1 rutile TiO<sub>2</sub> (110) surface (3.56 eV) [1], indicating interfacial vacancies are somewhat stabilized relative to those

on the single crystal TiO<sub>2</sub> surface. Hence the constructed nanowire is a reasonable model to examine the impact of interfacial reducible sites on catalytic chemistry, without overestimating the role of O vacancies due to an unrealistic enhancement of their stability at the interface.

Furthermore, a 0.28 eV more stable state than originally reported was found for the singly water-adsorbed state c in the reaction schematic for hydrogen adsorbed at the interface leading to an oxygen vacancy (Fig. 4 in the section “3.1.2. TiO<sub>2-x</sub>/Pd Reduced Surface (O Vacancy)” [1]). Consequently, the relative energies for states c and d are updated (also since these states involve the TiO<sub>2-x</sub>/Pd interface) and the Figure is updated as Fig. 1 here. Removal of the water molecule from TiO<sub>2-x</sub>/Pd states c (Fig. 1) now costs 0.83–1.11 eV, leaving behind an oxygen vacancy (states d) (Table S1, step Xb). The energy cost is still consistent with the previous estimates reported over a rutile TiO<sub>2</sub> (110) surface [2]. Also, as with the change in O vacancy formation energy, the cost to create a vacancy from the hydroxylated surface (state d relative to state a, Fig. 1) is 1.06 eV (without water co-adsorbed) against the earlier reported value of 1.62 eV. The corresponding cost with a water molecule co-adsorbed at the interface is still 0.96 eV. The updating of the energetics in this figure does not affect any conclusions or discussion in the original manuscript.

From section “3.2.1. Direct Deoxygenation (DDO)” of the paper, potential energy surfaces (PES) of DDO paths across DFT models in Fig. 5 [1] have been corrected for the adsorption energy of furfuryl alcohol at the TiO<sub>2-x</sub>/Pd interface to –2.06 eV (Fig. 2), correcting the earlier reported value of –2.66 eV. The Figure has also been corrected for the adsorption of the molecule oriented vertically to the surface (labelled “TiO<sub>2-x</sub>/Pd (O Vacancy), upright”). Similarly, in the section “3.2.3. Decarbonylation”, the potential energy surfaces (PES) of DCO paths across DFT models in Fig. 10 [1] have been corrected (Fig. 3) for the adsorption energy of the acyl intermediate C<sub>4</sub>H<sub>3</sub>O(CO)\* relative to the energy of gas phase furfural minus ½ H<sub>2</sub> and the new (corrected) energy of the bare TiO<sub>2-x</sub>/Pd surface. These changes do not affect the DDO or decarbonylation activation barriers or the reaction energies over this surface as neither reaction states involve a bare TiO<sub>2-x</sub>/Pd surface. As the conclusions reached in the paper regarding the rate of the DDO sequence were based on surface reaction activation barriers rather than

DOI of original article: <https://doi.org/10.1016/j.jcat.2019.07.012>

\* Corresponding author.

E-mail address: [mjanik@psu.edu](mailto:mjanik@psu.edu) (M.J. Janik).

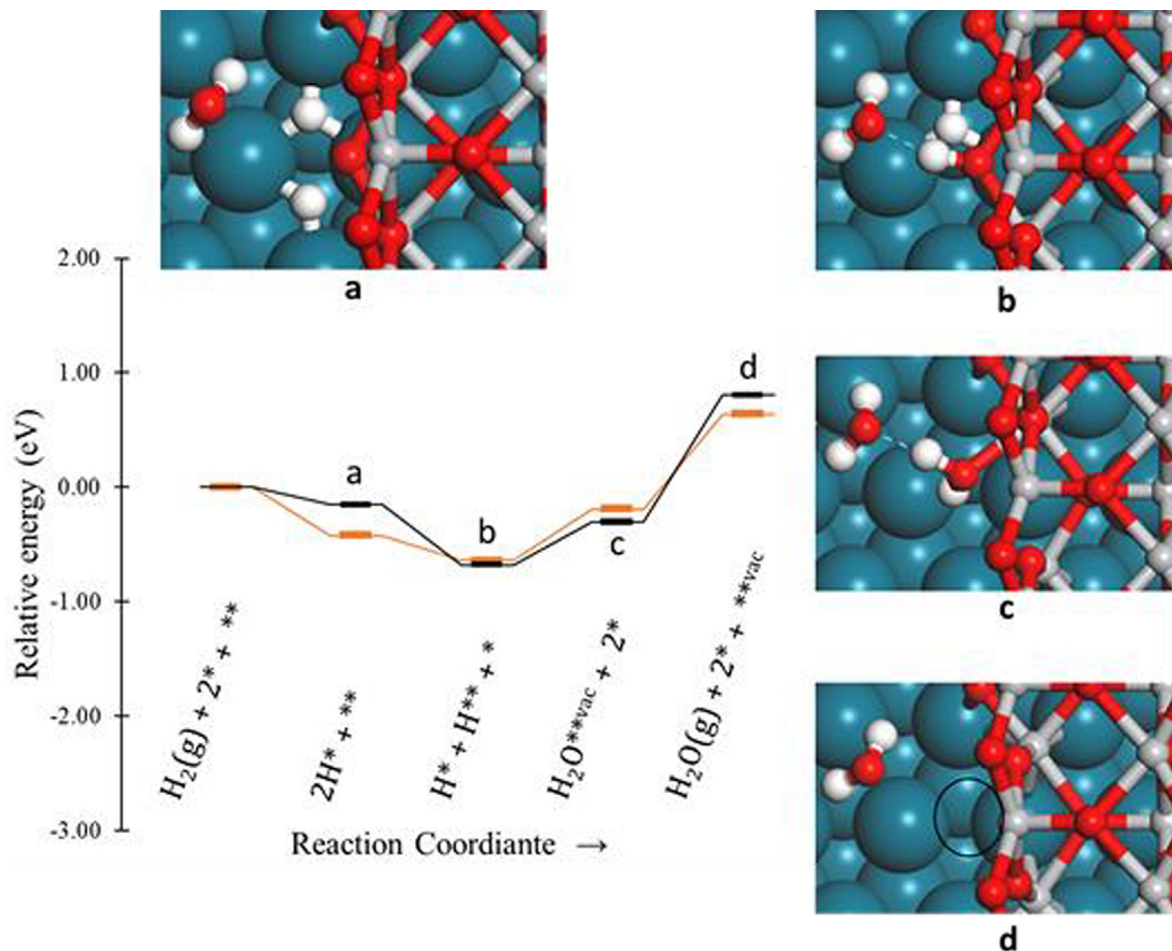


**Fig. 1.** Reaction scheme for hydrogen adsorbed at the interface leading to an oxygen vacancy with (-black) and without (- orange) the presence of water. Images show states along the vacancy formation process with an additional water molecule co-adsorbed. Blue dotted lines in states b and c show hydrogen bonding. \* , \*\* and \*\*\*<sub>vac</sub> refer to Pd sites, oxygen sites of TiO<sub>2</sub> and TiO<sub>2</sub> vacancy sites at the interface respectively. This Figure corrects Fig. 4 of Ref. [1].

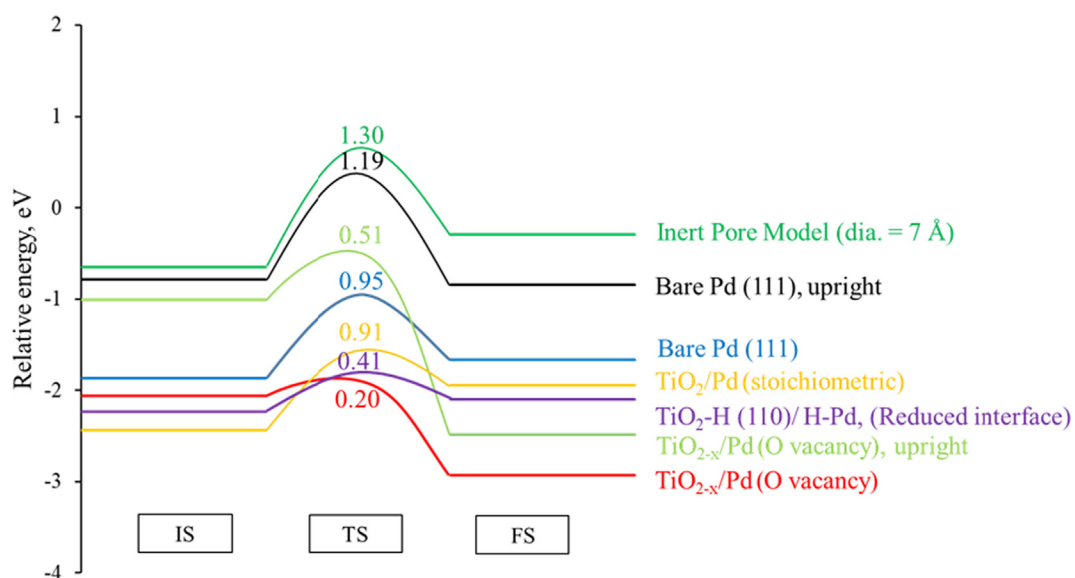


**Fig. 2.** Potential energy surfaces (PES) of DDO path over different DFT models as labelled. Initial and final state energies are plotted with respect to the energy of gas phase furfuryl alcohol and the respective surface models without adsorbed hydrocarbons. Activation energy barriers ( $E_a$ ) in electronvolts are labelled. Transition state structures are illustrated in Fig. 6 in Ref. [1]. This Figure corrects Fig. 5 of Ref. [1].

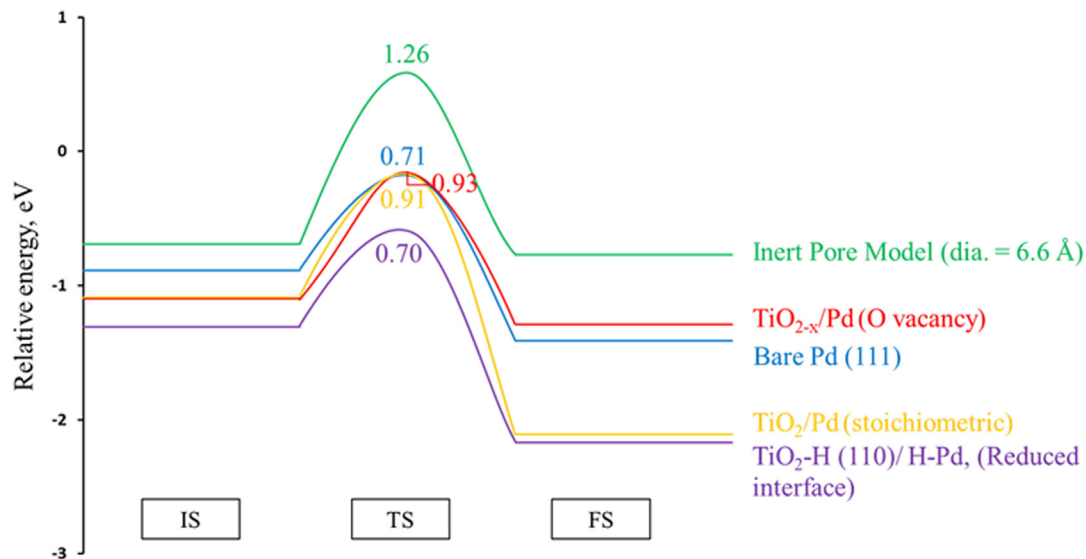


**Fig. 3.** Potential energy surfaces (PES) of DCO path over different DFT models. Initial and final state energies are plotted with respect to the energy of gas phase furfural minus  $\frac{1}{2} H_2$  and the respective surface models without hydrocarbons adsorbed. Activation energy barriers ( $E_a$ ) in electronvolts are labelled. Transition state structures are illustrated in Fig. 11 in Ref. [1]. This Figure corrects Fig. 10 of Ref. [1].

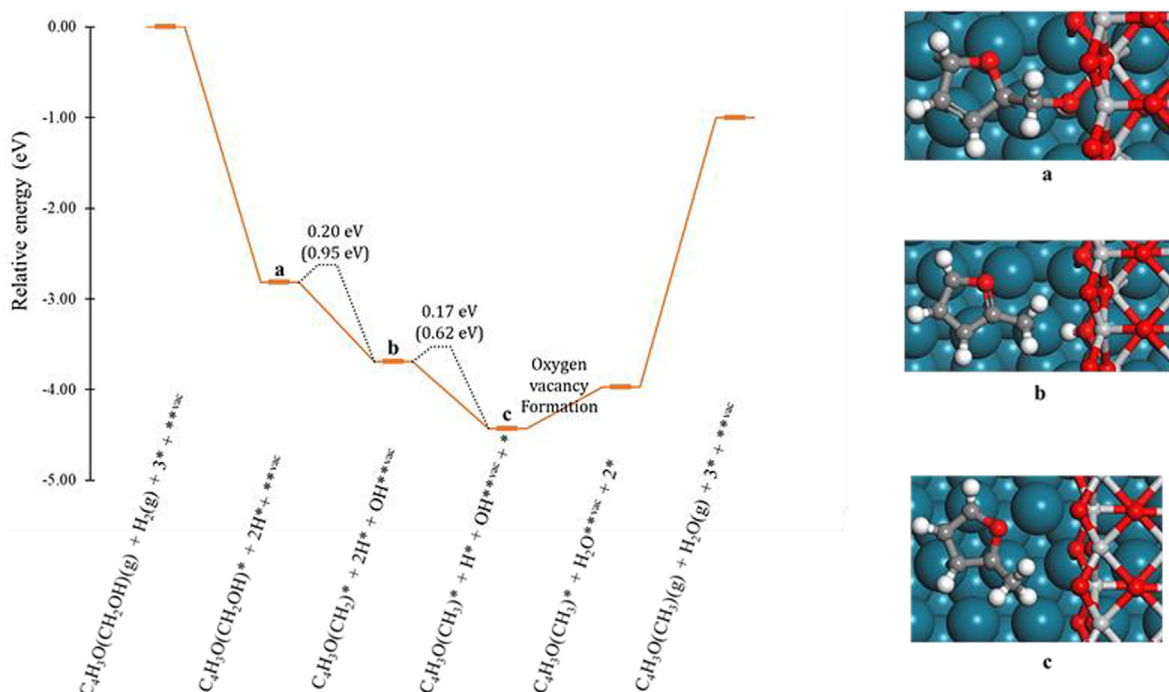


**Fig. 4.** Reaction energy diagram for DDO of furfuryl alcohol at a  $TiO_{2-x}/Pd$  reduced surface (oxygen deficient). The values in parentheses are the activation energies for corresponding steps over bare Pd (111). \* and \*\*vac refer to Pd sites and  $TiO_2$  vacancy sites at the interface, respectively. This Figure corrects Fig. 13 of Ref. [1].

adsorption energies, the changes to these results have no impact on these conclusions.

Finally, in section “3.3.2 DDO Mechanism:  $TiO_{2-x}/Pd$  Reduced Surface (Oxygen Deficient)”, Fig. 13 [1] showing a reaction energy diagram for the DDO of furfuryl alcohol has been corrected for the relative energies of states a, b, c and the later stages relative to gas phase furfuryl alcohol, hydrogen and the bare  $TiO_{2-x}/Pd$  surface ( $C_4H_5O(CH_2OH)(g) + H_2(g) + 3^* + ^{**vac}$ ) in Fig. 4. Consistent with the corrections elsewhere, there are no changes in activation barriers or desorption energies during the entire reaction schematic. As such, the major conclusion from our results is still valid, that in the presence of reduced  $Ti^{3+}$  sites and oxygen vacancies, the dissociation of the C—OH bond (direct deoxygenation) is thermo-

dynamically as well as kinetically far more feasible than that observed over the Pd (111) surface. Regeneration of these reduced active sites is also energetically feasible, completing the catalytic cycle.

The authors would like to apologise for any inconvenience caused.

## References

- [1] S. Deo, W. Medlin, E. Nikolla, M.J. Janik, Reaction paths for hydrodeoxygenation of furfuryl alcohol at  $TiO_2/Pd$  interfaces, J. Catal. 377 (2019) 28–40.
- [2] P.M. Kowalski, B. Meyer, D. Marx, Composition, structure, and stability of the rutile  $TiO_2(110)$  surface: Oxygen depletion, hydroxylation, hydrogen migration, and water adsorption, Phys. Rev. B 79 (2009) 115410.